2010

Image Segmentation and Analysis for Automated Classification of Traumatic Pelvic Injuries

Simina Vasilache
Virginia Commonwealth University

School of Engineering

Virginia Commonwealth University

This is to certify that the dissertation prepared by Simina Vasilache entitled IMAGE SEGMENTATION AND ANALYSIS FOR AUTOMATED CLASSIFICATION OF TRAUMATIC PELVIC INJURIES has been approved by her committee as satisfactory completion of the Dissertation requirement for the degree of Doctor of Philosophy

---

Kayvan Najarian, Ph.D., Committee Chair, Department of Computer Science

---

Krzysztof Cios, Ph.D., Department of Computer Science, School of Engineering

---

Vojislav Kecman, Ph.D., Department of Computer Science, School of Engineering

---

Rosalyn S. Hobson, Ph.D., Department of Electrical and Computer Engineering, School of Engineering

---

Toan Huynh, M.D., Carolinas Healthcare System

Kevin R. Ward, M.D., Department of Emergency Medicine, School of Medicine

---

Rosalyn S. Hobson, Ph.D.,Associate Dean of Graduate Studies, School of Engineering

---

Russell D. Jamison, Ph.D., Dean, School of Engineering

F. Douglas Boudinot, Ph.D., Dean of the School of Graduate Studies

---

Date

IMAGE SEGMENTATION AND ANALYSIS FOR AUTOMATED CLASSIFICATION OF TRAUMATIC PELVIC INJURIES

A dissertation submitted in partial fulfillment of the requirements for the degree of Doctor of Philosophy at Virginia Commonwealth University.

by

SIMINA VASILACHE

B.S., Academy of Economic Studies, Department of Cybernetics, Statistics and Economic Informatics (Bucharest, Romania), 2007

Director: KAYVAN NAJARIAN

ASSOCIATE PROFESSOR, DEPARTMENT OF COMPUTER SCIENCE

Virginia Commonwealth University

Richmond, Virginia

April, 2010

Acknowledgments

This material is based upon work supported by the National Science Foundation under Grant No.IIS0758410. The dataset used for this project was provided by the Carolinas Healthcare System and the Medical College of Virginia (MCV). I would like to thank Dr. Toan Huynh for his great help during the process of data collection, and to acknowledge the active involvement in this research of Dr. Kevin Ward and Dr. Kayvan Najarian, representing the Virginia Commonwealth University Reanimation Engineering Shock (VCURES) center. I thank my adviser, Dr. Kayvan Najarian, and all my committee members for their guidance in pursuing my degree. Special thanks to Dr. Charles Cockrell for his invaluable help, Wenan Chen and Rebecca Smith for their work and for making our collaboration an extraordinary research experience. Most of all, I would like to thank my wonderful family and all my incredible friends for their love and support.

Table of Contents

List of Tables

List of Figures

Abstract

IMAGE SEGMENTATION AND ANALYSIS FOR AUTOMATED CLASSIFICATION OF TRAUMATIC PELVIC INJURIES

By Simina Vasilache, Ph.D.

A dissertation submitted in partial fulfillment of the requirements for the degree of Doctor of Philosophy at Virginia Commonwealth University.

Virginia Commonwealth University, 2010

Major Director: Kayvan Najarian
Associate Professor, Department of Computer Science

In the past decades, technical advances have allowed for the collection and storage of more types and larger quantities of medical data. The increase in the volume of existing medical data has increased the need for processing and analyzing such data. Medical data holds information that is invaluable for diagnostic as well as treatment planning purposes. Presently, a large portion of the data is not optimally used towards medical decisions because information contained in the data is inaccessible through simple human inspection, or traditional computational methods. In the field of trauma medicine, where caregivers are frequently confronted with situations where they need to make rapid decisions based on large amounts of information, the need for reliable, fast and automated computational methods for decision support systems is stringent. Such methods

could process and analyze, in a timely fashion, all available medical data and provide caretakers with recommendations/predictions for both patient diagnostic and treatment planning. Presently however, even extracting features that are known to be useful for diagnosis, like presence and location of hemorrhage and fracture, is not easily achievable in automatic manner.

Trauma is the main cause of death among Americans age 40 and younger, hence, it has become a national priority. A computer-aided decision making system capable of rapidly analyzing all data available for a patient and forming reliable recommendations for physicians can greatly impact the quality of care provided to patients. Such a system would also reduce the overall costs involved in patient care as it helps in optimizing the decisions, avoiding unnecessary procedures, and customizing treatments for individual patients. Among different types of trauma with a high impact on the lives of Americans, traumatic pelvic injuries, which often occur in motor vehicle accidents and in falls, have had a tremendous toll on both human lives and healthcare costs in the United States.

The present project has developed automated computational methods and algorithms to analyze pelvic CT images and extract significant features describing the severity of injuries. Such a step is of great importance as every CT scan consists of tens of slices that need to be closely examined. This method can automatically extract information hidden in CT images and therefore reduce the time of the examination. The method identifies and signals areas of potential abnormality and allows the user to decide upon the action to be taken (e.g. further examination of the image and/or area and neighboring images in the scan).

The project also initiates the design of a system that combines the features extracted from biomedical signals and images with information such as injury scores, injury mechanism and demographic

information in order to detect the presence and the severity of Traumatic Pelvic Injuries and to provide recommendations for diagnosis and treatment. The recommendations are provided in form of grammatical rules, allowing physicians to explore the reasoning behind these assessments.

Novelty and Contributions

The increasing volume of data and the technological advances in medical field, combined with the large volume of patients in trauma care units, result in a stringent need for efficient and accurate decision making. Computer-assisted decision making systems can help caregivers by providing predictions and treatment recommendations which can contribute to improvement of the accuracy of decisions and reducing of the time needed to reach a decision. Such systems can therefore impact the overall quality of healthcare and reduce the healthcare costs. Traumatic pelvic injuries need to be diagnosed and treated in a timely manner as they are often accompanied by complications, such as infected hematomas and blood clots that can move to the brain or lungs, which can occasionally result mortality or permanent disability.

Almost all existing decision making systems rely solely on demographic information and features extracted from averaged physiological data to create diagnosis and treatment recommendations. Including information extracted from medical images such as X-rays, CTs and MRIs is essential for improving the accuracy of a computer-aided decision making system. Additionally, more refined and better tailored recommendations could be generated if the information hidden in images is included. The large number of pelvic CT slices that need to be examined, the complexity of pelvic structures and the range of injuries pose a challenge for physicians in terms of rapidly and successfully establishing a diagnostic. An automated system could significantly reduce the time associated with examining medical data and increase the speed and reliability of medical decision making. However, automatically extracting relevant features from available medical data is not

trivial and poses several challenges. The focus of this dissertation is on improving the decision making process for Traumatic Pelvic Injuries and using automated processing of CT images for bone tissue segmentation and detection of hemorrhage. In another part of the project, features extracted from CT image analysis are combined with demographic and physiological information as well as features obtained from X-ray images (generated by a companion project) in order to derive recommendations in form of grammatical rules.

The method presented in this dissertation has several novel components, described below, that attempt to alleviate some of the challenges associated with automated processing and analysis of medical data.

1) An automated seed generation method which allows for the initialization of the seed growing method and the Snake model. Automated seed generation is vital to the success of the entire system as selecting a sufficiently large number of relevant seeds across multiple slices in a CT scan can be very time consuming via manual selection. The proposed method has designed a sequence of specialized image filtering methods and gray level thresholding for automated seed generation. The selected threshold is derived from the statistical properties of the gray level of the image. This method is explained in Chapter 2.

2) A hierarchical method that uses seed growing and Snake modeling to improve segmentation connectivity and edge smoothness. Seed growing and the Snake model are initialized via the proposed automated seed generation. Constrained growing criteria are applied in order to achieve improved connectivity while avoiding the inclusion of non-bone pixels in the region. Initialization of the Snake model is achieved based on the results of the preliminary

segmentation as well as template matching. This study proposes that the Snake modeling is more successful for pelvic CT segmentation when it is initialized on the outside of the bone rather than on the inside. This algorithm will be introduced in Chapters 2 and 3.

3) A method to label similar gray level regions that do not represent bone based on shape matching and object recognition. This method can be used to exclude regions that are not bone and erroneously appear in the segmentation results, despite the fact that their average gray level is similar to that of bone. Using this method, the algorithm incorporates constraints that relate to the the position and shape of bone formations in the CT slice. Regions segmented in the same gray level range as bone tissue are distinguished from bone by matching the segmentation result to a set of bone templates. The proposed method, which is explained in Chapters 3 and 4, proved to be robust during testing and even small changes in the segmentation result are signaled by corresponding changes in matching cost.

4) Relevant features from patient demographic and physiological data and features extracted from X-Ray and CT images are combined in order to form a grammatical rule base that assess the level of injuries and predict the outcome for each patient. This system, whose reasoning is transparent to physicians via the grammatical structure of rules, may assist physicians in diagnostic and treatment planning.

The proposed algorithm was tested using a number of CT images from a reasonably sized pool of patients with traumatic pelvic injuries. For generating the results presented in this dissertation a data set consisting of eleven patients each having between forty five and seventy five different

CT images was formed. The images for each patient were selected such that they capture the variation of anatomical structures within a CT scan and are within the same range of a CT scan within the group of patients. The results, presented in Chapter 7, show that the proposed system can potentially be utilized to better make use of the knowledge hidden in CT images.

CHAPTER 1 Introduction

1.1 Overview

This chapter is dedicated to justifying the need for computer-aided assisted trauma decision making systems, in particular for traumatic pelvic injuries, and providing an overview of the existing CT image analysis techniques. First, the role of CT images in diagnosis and decision making for critical pelvic injuries is briefly discussed. Then, a concise review of the existing methods used for processing and analysis of pelvic CT images is provided. The chapter ends with a high-level overview of the method proposed in this project.

1.2 Problem Statement

Traumatic injuries are the number one cause of death in the 40 year and below age group [37], [33]. A staggering total of four million years of potential life are cut short every year in the U.S due to traumatic injuries [37]. Over 15 million Americans suffer traumatic injuries caused by falls, motor vehicle crashes and firearms each year. More potential life is lost to traumatic injuries than to cancer and heart disease [33] as 40% of fatal traumatic injury cases die before even reaching the emergency room [10]. The World Health Organization (WHO) estimates that by 2020 traumatic injury will surpass infectious diseases and become the leading cause of death worldwide [33]. Among the causes of traumatic injuries, motor vehicle crashes account for 48% to 68% of such

injuries and within traumatic injuries, traumatic pelvic injuries and associated complications, such as internal hemorrhage, infected hematomas, multi-organ failure and blood clots traveling to the brain or lungs, result in a mortality rate ranging from 8.6% to 50% [59]. Even when the injury is not fatal it is often the cause of life long disabilities [4]. Computer-aided decision making systems can improve trauma by increasing accuracy and reducing time for decision making. Such effects can, in turn, lead to improved healthcare standards, better resource allocation and lower healthcare costs.

Trauma decision making is extremely time sensitive; therefore, a decrease in decision making time can have a tremendous impact on patient care and treatment. Because traumatic injuries are often associated with specific causes, incidents of fatality or long-term disability may be avoided or reduced by making more accurate and timely decisions in trauma units [16]. As such, during the last few decades, a number of computer-assisted decision making systems have been introduced to address this need.

Although several computer-assisted trauma decision making systems already exist, the majority of these systems rely mainly on finding similarities between demographics of the patient being treated and those of past cases in trauma databases to provide a recommendation based on the outcome of these cases. As a result, the recommendations may not be accurate or specific enough for the purpose of practical implementation [16]. In the application addressed in this project, i.e. traumatic pelvic injuries, detecting the presence and severity of fractures and/or hemorrhage is an important step in assessing the injury severity. However, none of the existing systems consider the wealth of information contained in the images to predict outcome, despite such images being captured in civilian and military hospitals for practically all trauma patients. Existing systems consequently ignore the most important and relevant information regarding the injury, and there-

fore lack the accuracy and specificity expected from reliable computer-assisted medical decision making methods. For diagnosing traumatic pelvic injuries, often both X-ray and Computed Tomography (CT) of the pelvic region are taken and analyzed. Typically X-ray images are used as a preliminary step to discover the presence of clear and major injuries while more specific and detailed information can be perceived in CT scans due to their higher resolution. For instance, subtle fractures, such as fractures of the acetabulum and hip displacement, and presence of hemorrhage are typically assessed based on the analysis of CT images.

During a CT scan of the pelvic region, several 2D images of the transversal plane are generated, each spaced within a few centimeters of each other depending on resolution, are generated. Aligning these 2D images on top of each other as consecutive slices forms a 3D anatomical representation of the pelvic region. Since the number of CT slices / images can be large and each slice contains a significant amount of information, it is imperative to develop a computer-aided decision making system to extract all diagnostically important information from the scan. It is believed that a relatively small portion of the scan contains important information in terms of establishing a diagnostic decision [53]; importantly in some cases, such information may not be easily perceived by the human eye.

Due to the abundance of detailed information in CT images and the fact that more and more healthcare systems now use CT as the gold standard for diagnosis of pelvic injuries, this project focuses only on the processing of CT images and the extraction of diagnostically important information from these images.

The next section briefly describes the CT modality and its data characteristics for this imaging modality.

1.3 Computed Tomography (CT)

The technology for CT image acquisition was developed in the early 70's and gradually became a standard in a variety of clinical applications and settings. CT imaging uses X-ray energy to create a series of two dimensional transversal images of the body. The radiation that passes through the body is measured by detectors placed on the opposite sides of the body, across the X-ray transmitters. The image is reconstructed based on the principles of the Fourier Slice Theorem, which states that the internal structure of the irradiated object can be recreated from multiple X-ray projections. Every CT slice is composed of a large number of pixels that are associated with the attenuation values of the tissue located at the corresponding points. These values are calculated based on multiple intensity readings of the radiation that passes through the tissue during the CT scan, as described by the Fourier Slice Theorem.

The average of these multiple attenuation values for an element / pixel will constitute a numeric measure that is associated with a pixel in the CT image. This average value is measured in units, named after the inventor of the first CT machine, Sir Godfrey Hounsfield. The dynamic range of a Hounsfield unit (HU) is 2000 units, increasing to 4000 or more in modern CT scanners. The range of attenuation is typically divided as follows: air -1000, lung tissue -400 to -600, fat tissue -60 to -100, water 0, soft tissue 40 to 80 and bone 400 to 1000.

The the human eye may not be able to distinguish between such a large number of gray level values, and a computer would therefore perform better in discerning to which category of tissue a certain pixel needs to be allocated. However, it is difficult even for a computer to assign a pixel to a tissue class solely based on its HU value, as the CT image is affected by noise, partial volume effects, in-homogeneity, and other factors.

Much more information is needed in order to associate a pixel with a particular anatomical region. For instance, the spacial proximity of pixels to each other constitutes an important criterion in assigning neighboring pixels to the same structure. The art of considering all information in the image and assigning a label to each pixel, in other words identifying the region it belongs to, forms an important branch of digital image processing called “segmentation”. In order to analyze any biomedical image, it is essential to first segment the image. The next section describes different segmentation methods used for biomedical images, in particular CT.

1.4 Image Segmentation

Formally speaking, image segmentation is the task of partitioning an image into disjoint regions that are homogeneous according to some predefined criteria [38]. A segmentation algorithm must ensure that after segmentation the following conditions are met:

1. The surface that is to be segmented is fully covered by the resulting partitions,

2. The segmented regions are disjoint, and

3. Points in a region are connected as defined by a pre-established criterion.

If the last condition is removed the task becomes one of pixel classification. Two typical challenges encountered in biomedical image segmentation are: partial volume effects and intensity inhomogeneities. A short description of these two common problems is as follows:

1. Partial volume effects. These occur at the boundary between tissues, where more than one type of tissue contributes to the intensity of a pixel [49], [56], [41]. The image artifacts

caused by partial volume effects blur tissue boundaries, complicating the task of tissue delineation. Partial volume effects are an intrinsic limitation of all image modalities, and image processing methods cannot entirely eliminate their deteriorating impact on image segmentation. A common approach to the problem is “soft segmentation”, which allows for a certain degree of uncertainty at the boundary where two regions overlap [38].

2. Intensity inhomogeneities. Regardless of the exact choice of imaging technology used to form an image, it is known that due to tissue inhomogeneities and the pixels belonging to the same class of tissue vary in intensity. In other words, there is no constant intensity value that can uniformly characterize a tissue.

To address the specific challenges in segmenting biomedical images, including the two described above, highly specialized segmentation methods have been developed and have been applied in CT imaging processing. These methods are reviewed in the following subsection.

1.4.1 Biomedical Image Segmentation Methods

Several categories of methods for medical image segmentation are presented in the literature of biomedical image processing [38]. Other more recently introduced groups of biomedical image segmentation methods, are not thoroughly discussed and compared with others in detail. All of these methods will also be surveyed and presented below.

1. Thresholding methods: Segmentation methods based on thresholding [44], [45], [24] view the segmentation task as a pixel classification problem. Such techniques produce a binary partition of the image based on the characteristics of each pixel individually, often

using a pre-established threshold. If the observed characteristic, most commonly the gray level value, meets a specified condition relating to the pre-defined threshold, the pixel will be categorized accordingly. Thresholding techniques are very simple to implement and provide fast results. However, choosing a proper value for the threshold is not trivial and it is not uncommon that the pixels in the ideal segmented region cannot be uniformly and uniquely characterized by a single threshold value.

2. Region growing: Region growing segmentation techniques [35], [31], [1], [26], [36], [39], [28], are very popular in medical image segmentation. The general approach is to start from an initial set of seed points and proceed by adding new points to the region which meet a certain similarity criterion. Region growing techniques are simple and effective in achieving correct segmentation for many applications. Such methods rely on simple concepts and are generally not difficult to implement. However, they pose certain challenges in choosing initial seeds and establishing a similarity criterion. The task of choosing the initial seeds can be accomplished by manual selection, semi-automated selection, or fully-automated selection.

   (a) Manual selection implies a considerable level of human involvement. I is therefore susceptible to human subjectivity in choosing appropriate seeds and can be very time-consuming.

   (b) Semi-automated selection requires less human involvement in the selection stage as a smaller portion of seed points are selected manually. However, the method demands more effort in the search for suitable seeds based on a chosen criteria. Often the search process involves further human interaction in eliminating automatically gen-

erated seeds that are not considered suitable by the human expert.

(c) Fully-automated selection requires the least amount of human involvement and is faster. However, the fully-automated method requires for significant effort in the algorithm design stage.

It must be mentioned that, regardless of the exact method deployed for initial seed selection, region growing methods are sensitive to the initial choice of seeds and different seeding may produce different segmentation results. The second major challenge of the region growing method is choosing the similarity criteria. Such a task is even more complicated than the choice of the seeds. This is due to the fact that the similarity measure may not be apparent by visual inspection, and must therefore be determined via calculation of various statistics of the characteristics of the points and neighborhoods. Additionally, classic region growing methods are dominated by the growth of the current region. Keeping these aspects in mind, region growing methods are simple techniques that generally provide relatively good results once the above-mentioned challenges are properly addressed.

3. Clustering methods: Clustering segmentation methods [69], [25], [2] create clusters which segment the target image into regions. Both agglomerative and divisive approaches are used to accomplish this task. The main challenges that are faced in segmentation by clustering are finding the correct number of clusters, and choosing the appropriate inter- and intra-cluster distances. The problem of determining the number of clusters becomes more simple for the case of biomedical image segmentation applications, as it can typically be decided based on domain knowledge. However, the task of finding the appropriate inter- and intra-cluster distances is more challenging. Inter-cluster distance is necessary to determine the

cases in which similar, neighboring clusters can be merged in agglomerative clustering, or when a cluster needs to be split into multiple other clusters in divisive clustering. Various image characteristics can be incorporated in defining these distances texture information and gray level values are the most commonly used factors. Disadvantages of clustering methods include the following:

(a) Resulting regions may not be replicable over different runs of the algorithm.

(b) When clusters include a large number of pixels the algorithm becomes computationally expensive due to calculation of distances. A challenge that is prevalent in bone segmentation for all image modalities, in particular CT images, comes from the fact that bone density typically varies across a single structure and therefore a large number of pixels that should be clustered as bone will be assigned to other clusters.

4. Markov Random Field Models: The main contextual constraint made by Markov Random Field (MRF) [50] is that neighboring pixels are expected to belong to the same region [55]. This assumption forms a field, F, in which the filed value at each point is associated with one of the labels. Specifically, F can be viewed as a field of random variables among which the Markov conditions hold, i.e. only neighboring pixels have direct interactions with each other, and non-neighboring pixels are conditionally independent. The probability distribution of such a field, i.e. $P(F)$, is known to obey the Gibbs distribution [65]:

$$P(F) = \frac{1}{Z} e^{-U(F)} \tag{1.1}$$

where Z is the partition function which is the same for different F and is often defined for each image segmentation application according to its specific needs, and $U(F)$ is a priori

energy function. While MRF methods have shown great potential in image segmentation applications [5], their main disadvantage of MRF-based methods is that the energy function associated with most non-trivial MRF problems is extremely non-convex, and as such, the minimization problem is computationally expensive and time-consuming. In order to reduce the computational burden associated with typical MRF applications, some hybrid approaches using multi-resolution techniques have been proposed [42], [22] which begin by processing images at a coarse resolution and then progressively refine them to a higher resolution [68].

5. Region formation using deformable models: Deformable models [8], [51], [20], [30], [67], [52], [43], [21] are parametric methods which make use of closed curves that deform under internal and external forces in order to create a region. The initial curve is placed in the vicinity of the boundary of the region to be segmented, in order to ensure acceptable convergence to the boundary. The initial curve can be placed inside or outside of the region to segment. The curve is then iteratively deformed and moves outward or inward towards the boundary, depending on the choice of initial placement. The internal forces associated with the curve regulate its smoothness and the external forces attract it towards the boundary of the region. Deformable models are sensitive to the placement of the initial curve, require a significant amount of computational effort and generally have poor convergence towards concave boundaries.

6. Atlas-guided segmentation: These approaches are applicable when a segmentation template exists or can be created [12], [46]. Atlas segmentation is more feasible for segmentation of structures that do not exhibit great variation and are not extremely detailed or intricate.

When using such approaches probability models or manual land-marking can be used, in order to counteract variability. Generally these methods rely on registration methods to form a correspondence between the image to be segmented and the selected template. Their intrinsic advantage is that after segmentation is completed, a labeling of the segmented regions is available.

7. Watershed method: There are several watershed algorithms used for medical image segmentation [53], [48], [57], [27]. Watershed methods achieve segmentation of an image by splitting the image into different regions based on the topological features of the image gradient. The underlying idea is to start with an initial set of points where flooding begins and gradually form catchment basins. When two catchment basins originating from different sources meet, the algorithm stops. The problem that prevails in classic watershed algorithms is over-segmentation. Often images that need to be segmented are noisy; in medical images this is almost always the case. Noise can impact classic watershed algorithms by creating a large number of local minima which in turn can lead to over-segmentation. There are a number of approaches which address this problem, one of the most popular being marker-based watershed segmentation. This method assumes that markers are placed inside the image to be segmented and only these markers become flooding sources as opposed to all of the local minima. Another popular approach is to perform filtering for noise reduction before deploying the watershed algorithm; this can also be done through multi-resolution image representation and filtering [14]. Despite all these strategies, watershed is known to over-segment images and therefore is not a very popular segmentation method for many types of biomedical images.

8. Level set methods: Another category of segmentation for medical imaging is the family of level set methods [47], [54], [34], [70], [58], [66], [23]. Introduced in 1987 by Osher and Sethian [34], the level set method has proved its applicability in image segmentation. The level set of a real function is a set of points where the function takes on a pre-established constant value. Level set methods (LSM) define a level set function over a regular grid and assume the initial curve to be the zero level set. The initial curve is iteratively deformed according to the solution given by a set of partial differential equations (PDEs) towards better segmentation of the desired contour. There are different approaches for evolving the initial curve. One approach is to update the curve globally while another is to perform local updates by windowing the neighborhood of the level-set and updating only the PDEs that fall into the windowed space. Although LSMs have gained popularity in image processing over the years, their drawbacks have limited the use of such methods in many biomedical applications. Their main disadvantage is the fact that sophisticated and complex calculations are required to solve the level set partial differential equations. These calculations are often time-consuming and may not converge to the best result.

1.5 Proposed Method

The method proposed in this dissertation is a multi-stage hierarchical technique which applies the capabilities of improved versions of a combination of some of the methods discussed above. In particular, the proposed algorithm provides a novel approach in the automated seed initialization, the formation of a deformable model, and the growth of the model to form a region. A multi-stage pre-processing technique is also introduced to deal with variations typically observed in biomedical images.

The ultimate goal of the algorithm is to segment CT images of the pelvis and extract features that can be aggregated into recommendation rules for use in diagnosis and treatment planning. An overall schematic diagram of the modules of the algorithm is presented in Figure 1.1.

The algorithm individually analyzes each CT slice in the scan sequence as follows: First, the abdominal region is extracted and an initial bone segmentation is achieved through adaptive gray level thresholding and seed growing. Next, the resulting preliminary bone segmentation is compared to a set of manually created templates and an association is formed between the segmentation image and the most appropriate template. Identifying the template that best matches the segmentation allows the algorithm to more precisely determine the exact section of the scan that is being examined. Using the preliminary segmentation result and the matched template, a refined bone segmentation is created. The preliminary segmentation is also used to automatically initialize a Snake model. The Snake approach is used due to its ability to generate closed contours, and so provide better connectivity in the segmentation process while maintaining a close distance to the edges. After bone segmentation is refined potentially useful features are extracted. These are combined with features extracted from X-ray images, created by a companion project, and physiological and demographic information to form a dataset used for classification. Preliminary results of classification have placed CT image features among the top nodes of the decision trees, which suggests that the ability to automatically extract features from medical images is vital for the development of an accurate computer-aided decision making system.

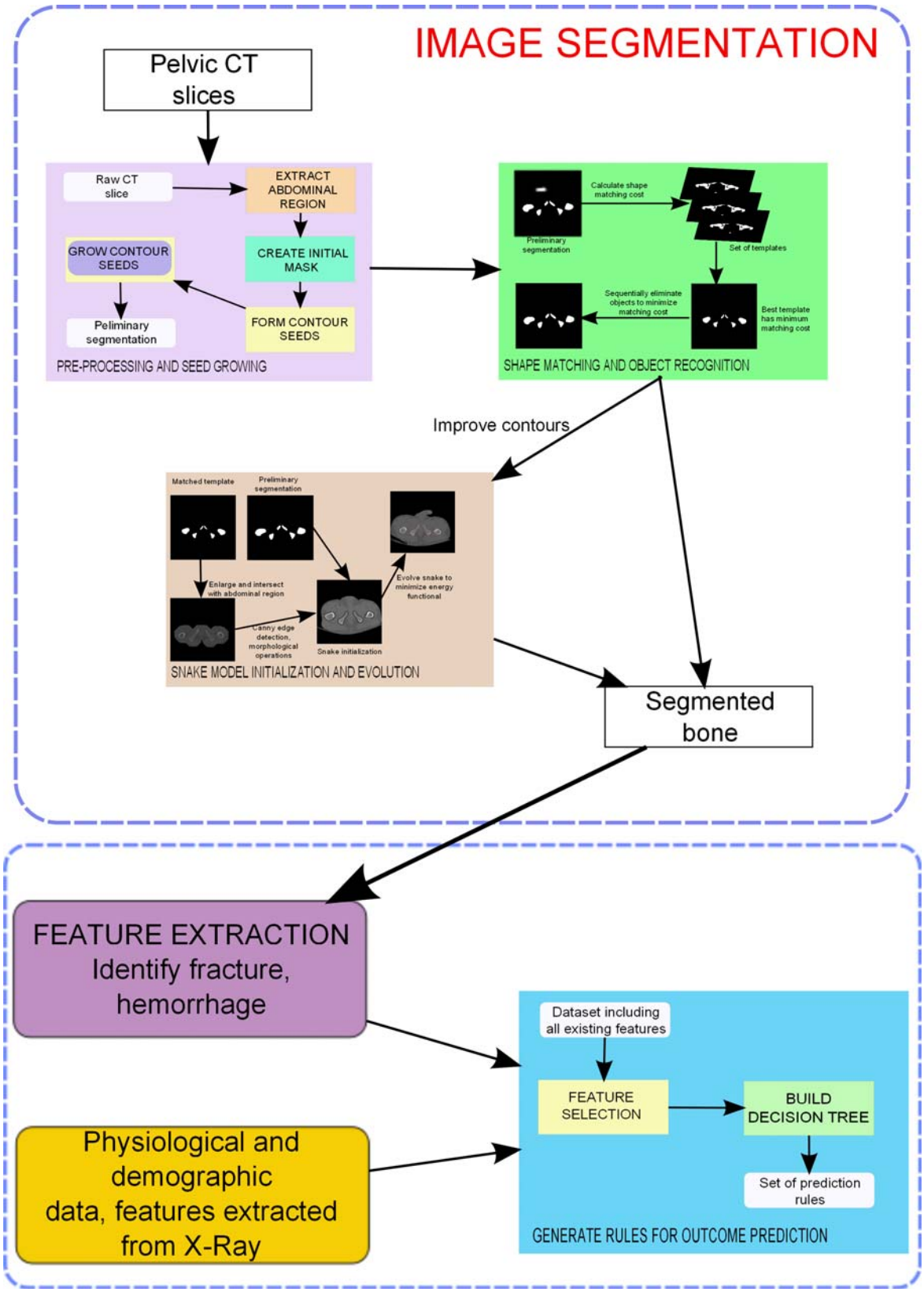

Figure 1.1: Algorithm Overview.

CHAPTER 2 Methods for Pre-processing and Seed Growing

2.1 Overview

The pre-processing and seed growing components of the system perform the initial segmentation of a single CT slice, remove artifacts and produce a set of regions that are candidate bone objects. Before creating the contours for any region, bone or blood, it is necessary to filter and pre-process raw images, and generate seeds to be grown in order to form the final candidate regions[1]. Seed selection and seed growing are extremely important for segmentation. Approaches towards initial seed selection include manual selection, semi-automated selection and fully automated selection. In any of these approaches there is a trade-off between human interaction and ease of implementation. The solution for initial seed selection presented here is fully automated. Segmentation of pelvic CT images assumes processing of several tens of images from a single CT scan. It is extremely time consuming for an expert to have to manually select relevant initial seed points in all the slices of the scan.

This chapter describes the proposed hierarchical pre-processing and seed growing methodologies. An overall schematic diagram for the components involved in pre-processing and seed growing can be seen in Figure 2.1. Part of the methods and ideas presented in this chapter were published in [61] and [63].

[1] "region" and "object" are used interchangeably throughout this dissertation

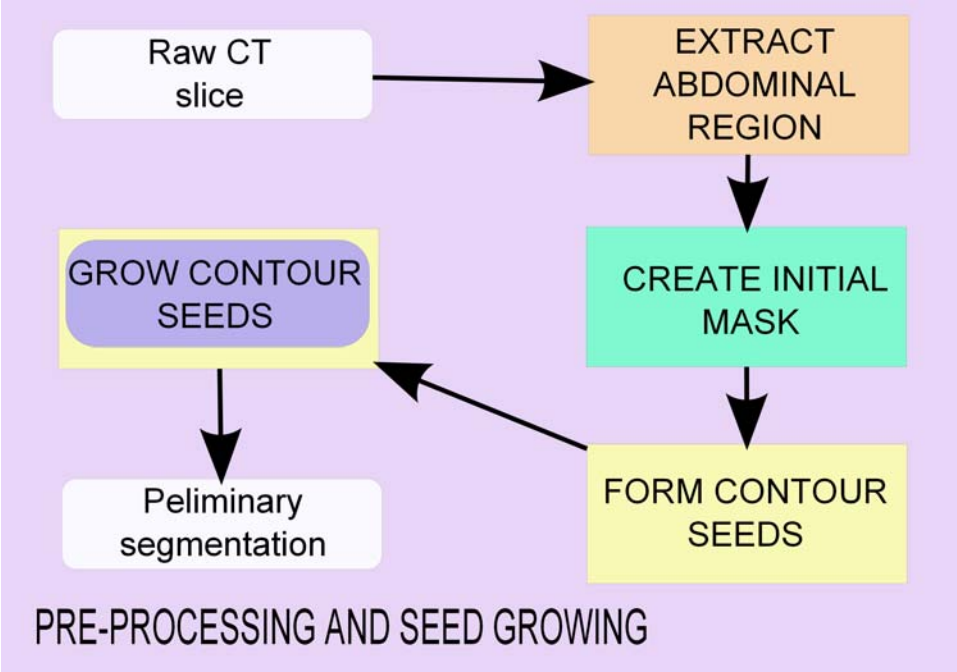

Figure 2.1: Pre-processing and seed growing overview.

2.2 Pre-processing

The ultimate goal of the pre-processing step is to separate the image of the main subject, in this case the pelvic region, from the irrelevant objects present in the image. More specifically, the proposed pre-processing method distinguishes between the pelvic region and the irrelevant nearby artifacts such as the CT table, cabling and the lower extremities that are visible in most CT images. A schematic diagram for this stage of the algorithm is provided in Figure 2.2.

To accomplish the segmentation of the pelvic region from these objects that constitute the background the following pre-processing steps are implemented:

Step 1: Create a binary version of the raw image. All the pixels whose gray level is higher than an adaptive threshold are set to one. Pixels with gray value smaller than the same threshold

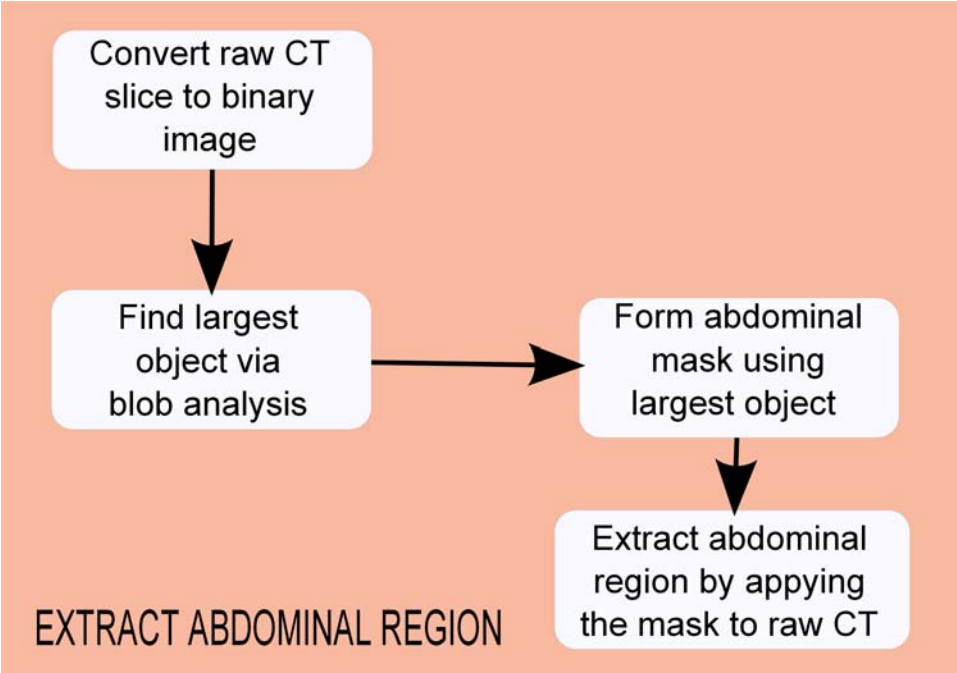

Figure 2.2: Diagram for the pre-processing (Abdominal Region Extraction) stage.

become zero in the new image. The abdominal region and some of the surrounding artifacts have a higher gray level value than the background. Such a characteristic allows thresholding to create a binary image in which the abdominal region and some of the artifacts are well separated from the background.

Step 2: Apply morphological operations to the binary image so that different objects in the image are separated. The region of interest is the pelvic region but as previously mentioned the image captures cabling and additional artifacts. Morphological operations help disconnect components in the image and allow for selection of the pelvic region in the next step of the algorithm.

Step 3: Use blob analysis to select the object that has the largest area. In this step general statis-

tics, such as area and center of mass, of each object in the image are computed and the object with the largest area is selected. This selection is based on the knowledge that all the individual artifacts have smaller areas than that of the pelvic region.

Step 4: Create a mask that is the size and shape of the object identified in Step 3. The mask created so will help select the pelvic region from the initial image and eliminate irrelevant background artifacts.

In order to visualize the results produced by this series of steps, some example results are provided in Figure 2.3. Notice how in 3(b) and 3(d) the CT table and surrounding artifacts were eliminated, compared to the corresponding raw images presented in 3(a) and 3(c).

2.3 Initial Bone Mask Formation

Once the pelvic region is extracted and the background is removed from the image, the algorithm focuses on segmentation of bone. From now on the image of the pelvic region will be referred to as the original image. The schematic diagram that outlines this portion of the algorithm is presented in Figure 2.4.

Sample results for each of the components will be provided below. For consistency, the same set of images that was used in the pre-processing section will be used throughout the rest of the process.

The steps to obtain the initial segmentation are as follows:

Step 1: Apply Wavelet analysis and reconstruct the image using only the approximation matrix. Wavelet analysis is performed on the original image - the abdominal region image resulted

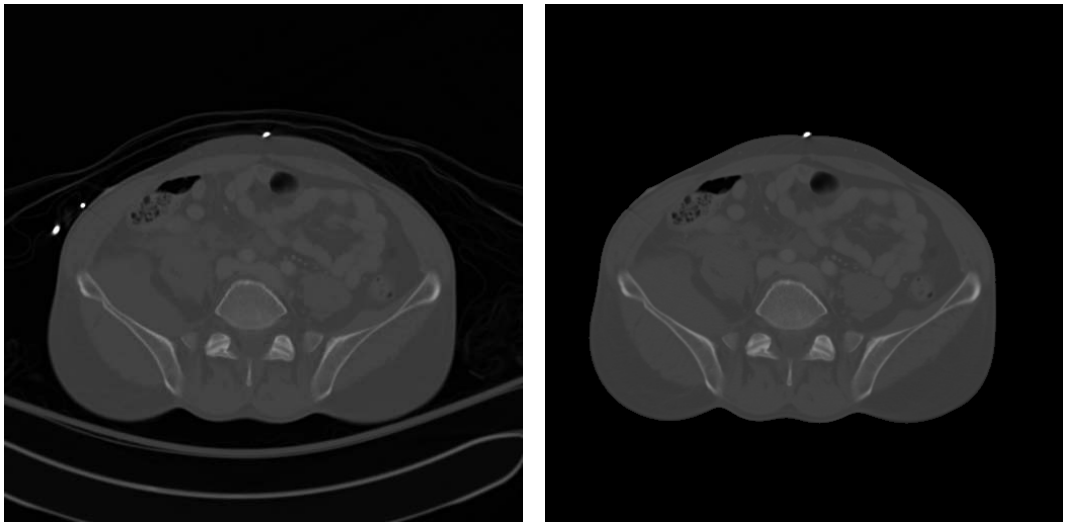

(a) Raw CT slice example A.

(b) Abdominal Region corresponding to Raw CT example A.

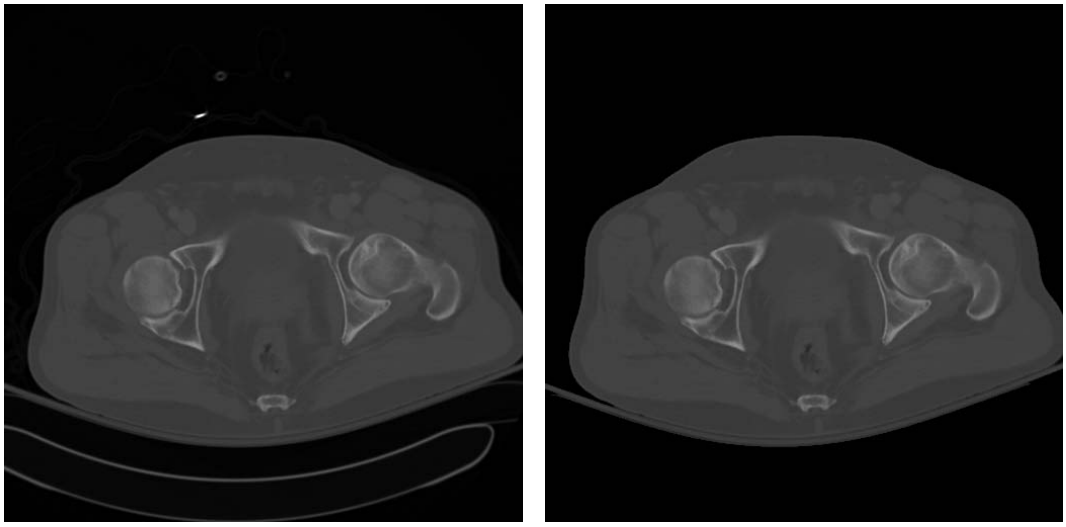

(c) Raw CT slice example B.

(d) Abdominal Region corresponding to Raw CT example B.

Figure 2.3: Example results for Abdominal Region Extraction.

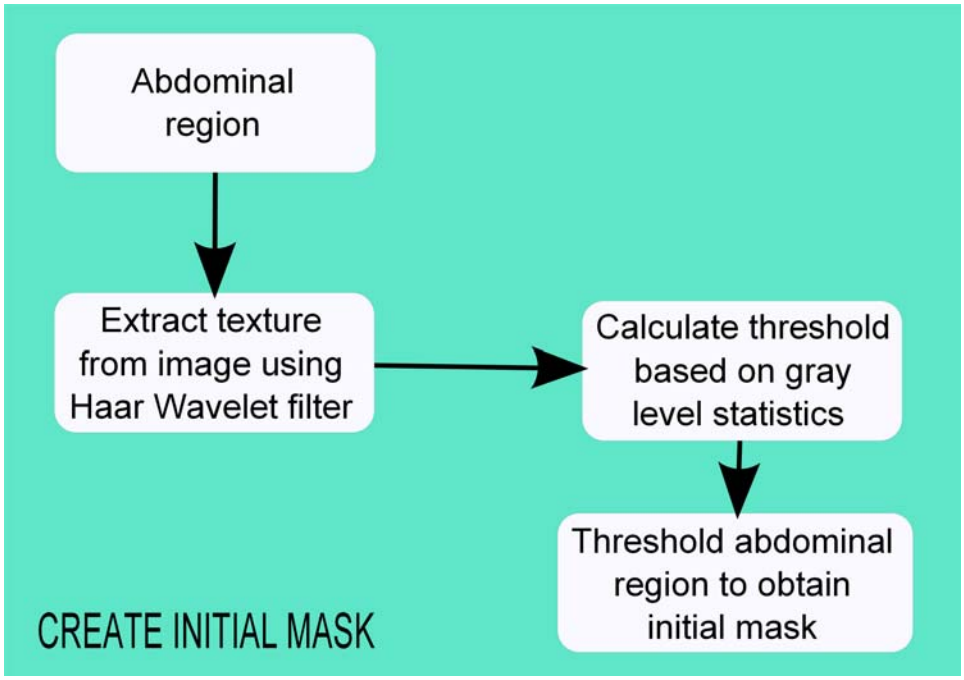

Figure 2.4: Diagram for the Initial Bone Mask Formation stage.

from the previous step. Haar wavelet is chosen for the mother wavelet in the analysis. The CT image exhibits sudden changes in gray level at the boundaries between different types of tissue. Therefore it calls for a mother wavelet that is described by a discontinuous function to facilitate processing and eliminating the discontinuities in gray level. As such, Haar wavelet was selected because of its discontinuity and intrinsic ability to accentuate transitions between gray levels. Assuming that I is a $2x2$ window of the abdominal image and W is a $2x2$ window of the wavelet filtered image then:

$$W = HIH^T \tag{2.1}$$

where

$$H = \frac{1}{\sqrt{2}} \begin{bmatrix} 1 & 1 \\ 1 & -1 \end{bmatrix}$$

This step is important for eliminating some of the texture in the CT image while preserving some of the discontinuities representing the edges.

Step 2: Calculate the means and deviation of the gray scale values of the pixels that are not background. The pixels that are not background are the pixels that fall within the masked region. The means and deviation of the gray level values are used in Step 3 for automatic threshold selection. It is important to focus only on the pixels that fall within the masked region since the CT image contains a significant number of background pixels. Including background pixels in the calculations can greatly distort the gray level statistical properties of the pelvic region.

Step 3: Calculate threshold value as the sum of means and standard deviation of the gray scale values calculated at the previous step. The threshold value t_1 is defined as the sum between the modified means m_1 and standard deviation st_1 of the gray values of the pixels that are not background. Specifically:

$$t_1 = m_1 + st_1 \tag{2.2}$$

where

$$m_1 = \frac{\Sigma_{x=0}^{N-1} \Sigma_{y=0}^{M-1} f(x,y)}{NM - Card(S)} \tag{2.3}$$

$$st_1 = \sqrt{\frac{\Sigma_{x=0}^{N-1}\Sigma_{y=0}^{M-1}(f(x,y)-m_1)^2}{NM - Card(S)}} \tag{2.4}$$

and

$$S = \{(x,y)|f(x,y) = 0\} \tag{2.5}$$

is the set of the pixels located in the background having zero gray level value. In addition, $Card(S)$ is the notation used here to denote the cardinality of set S.

Threshold selection can be a very challenging task especially since human eyes cannot distinguish between a wide range of gray levels and choose a suitable threshold value. Manual selection of multiple thresholds in a series of images can become extremely time consuming. It is important to design a method to automatically select suitable thresholds for an image. It was discovered, through experimental testing, that a threshold measure that is the sum between the average gray level and the standard deviation of the gray level values, as introduced above, is suitable.

Step 5: Create an initial binary mask for bone by thresholding the low pass image, i.e.

$$Mask_{Initial}(x,y) = \begin{cases} 1 & \text{if } f(x,y) \geq t_1; \\ 0 & \text{otherwise.} \end{cases}$$

This step produces an initial binary bone mask, selecting the pixels that have gray level values greater than the threshold identified in the previous step. Since the value of the threshold is the sum between average and standard deviation of the gray levels in the abdominal re-

gion, the pixels selected in this step have gray level values situated on the brighter end of the gray level spectrum. This increases the likelihood that the selected pixels have gray level values in the same range as bone tissue gray level values.

Establishing automatically which regions in the CT slice represent bone cannot solely rely on grey level information, as the range of gray level for bone overlaps with that of other tissues. To decrease the likelihood for regions that are far from the location of the bone in the slice, the result of the initial mask is intersected with an enlarged template. While analyzing a CT scan, the length of the CT scan is divided such that the slices to be examined are grouped into five sections. As such we can determine which section of the scan a current slice which is examined belongs to. The initial mask for the CT slice being analyzed is intersected with an enlarged bone template that corresponds to the current section. The set of five enlarged templates if formed as follows:

1. A set of one hundred bone templates was formed by manual segmentation of bones.
2. The set of templates is divided into five sections so that each section forms a subset of twenty ordered templates.
3. An enlarged template is formed by binary addition of the twenty templates in a section and dilation of the result.

Sample results for the Initial Bone Mask Formation stage are provided in Figure 2.5. As previously mentioned, the same set of images will be used throughout all examples for consistency purposes.

As it can be observed in Figures 5(b) and 5(d), the algorithm can produce a good initial bone segmentation, capturing size and location, through implementing the above-mentioned steps. How-

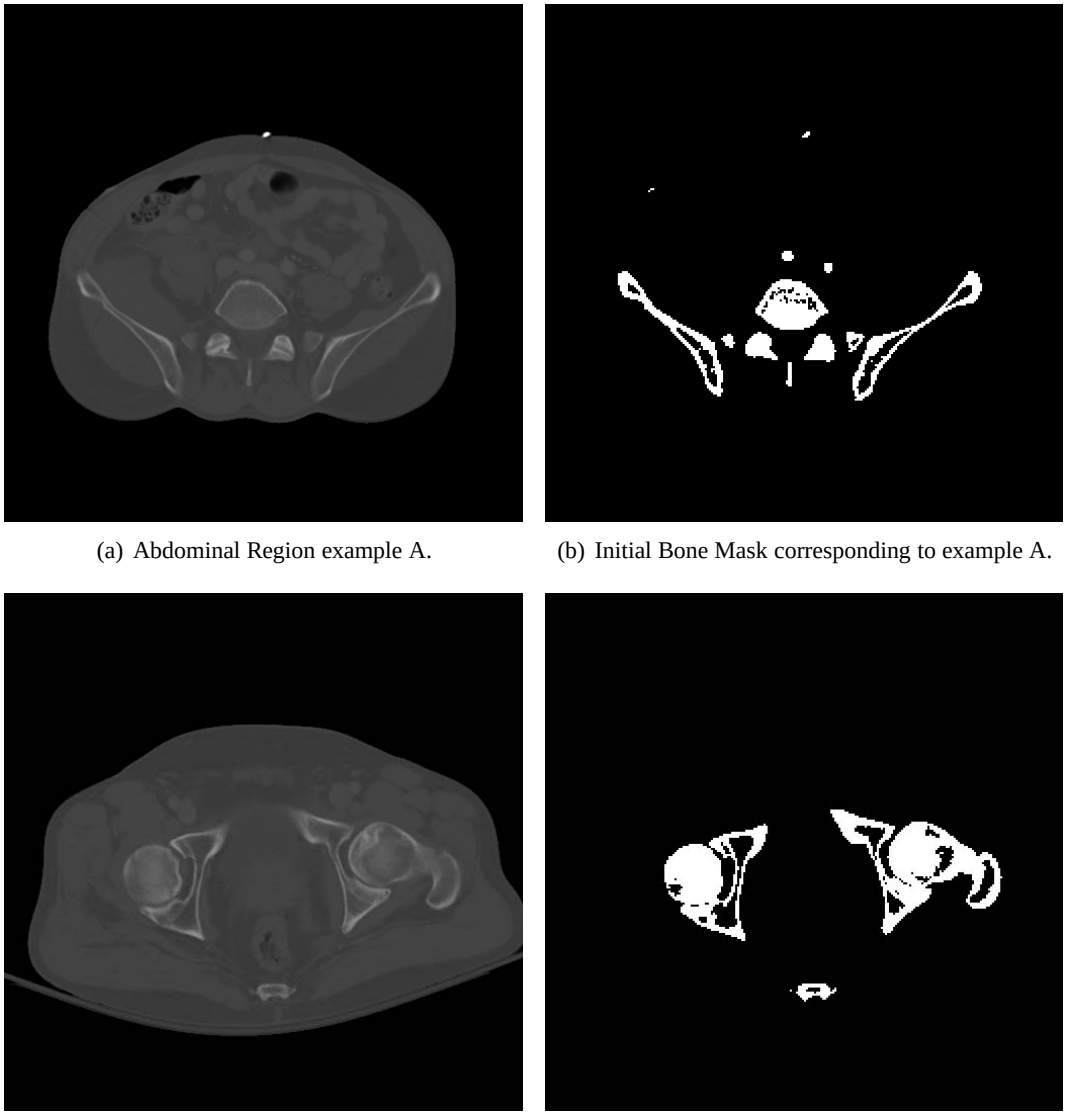

(a) Abdominal Region example A.

(b) Initial Bone Mask corresponding to example A.

(c) Abdominal Region example B.

(d) Initial Bone Mask corresponding to example B.

Figure 2.5: Example results for the Initial Bone Mask.

ever, further processing is needed: edges of the bones are not smooth, in the upper portion of the image bright regions that are not bone were captured, and other results show lack of connectivity in the segmented bones.

2.4 Forming Seeds Close to Contour

After obtaining the initial binary mask for bone, the mask is refined and an intermediary binary mask is created. In order to further improve the initial mask, a two dimensional Gaussian filter will be applied to the original image. The resulting image will appear smoother and texture will be eliminated. Eliminating texture will help create regions with more uniform gray levels, which is important considering the difficulty of performing segmentation caused by variations in gray level within the same tissue category. A schematic diagram presenting the steps taken at this stage of the algorithm is presented in Figure 2.6. A short description of the steps taken in this stage is given below.

Quantitatively speaking, in the process of obtaining the intermediary bone mask, a two dimensional Gaussian filter is applied to the original image. An one dimensional Gaussian filter is:

$$G(x) = \frac{1}{\sqrt{2\pi\sigma^2}} e^{-\frac{x^2}{2\sigma^2}} \tag{2.6}$$

For filtering of the image a 2D Gaussian filter is used. A 2D Gaussian filter is a product of two one dimensional Gaussian filters and is constructed based on the equations below:

$$G(x,y) = \frac{1}{2\pi\sigma^2} e^{-\frac{x^2+y^2}{2\sigma^2}} \tag{2.7}$$

where x and y are the distances from the origin on the horizontal and vertical axis, respectively, and σ is the standard deviation of the Gaussian. Given the original image and window size, a suitable

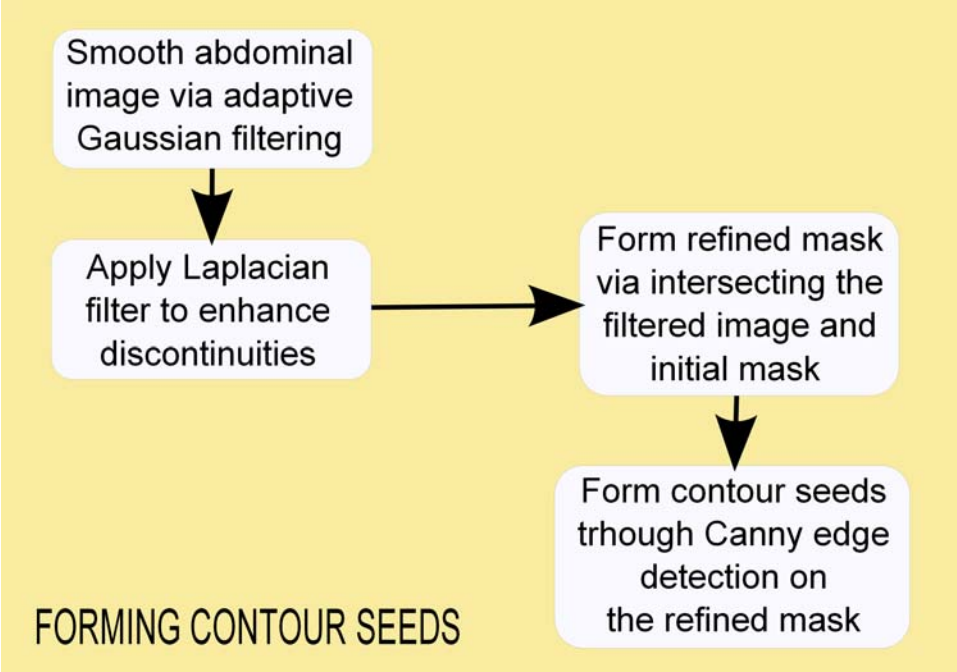

Figure 2.6: Diagram for Forming Seeds Close to Contour.

value for the σ parameter of the Gaussian filter is calculated. The parameter σ is calculated adaptively for each window, as described in [11], using a window of size $ws = 9$, the standard deviation of gray level inside the window and the standard deviation of noise in the image.

The lowpass filtering of the image is helpful in reducing the speckle noise that plagues CT images. Eliminating noise is a very important step as noise can affect local aspect and features of the structures of interest as well as reduce the overall quality of the image. The resulting image y_g gray values are given by:

$$y_g(x,y) = \frac{1}{2\pi\sigma^2} e^{-\frac{x^2+y^2}{2\sigma^2}} \tag{2.8}$$

After applying the Gaussian filter, a Laplacian filter is applied to the resulting image. The Laplacian filter will have the effect of capturing and enhancing vertical, horizontal and diagonal discontinuities, which translates into better defined edges.

An intermediary, refined bone mask is then obtained through binary multiplication of the initial binary mask and the filtered image.

Through Canny edge detection performed on the refined mask, seeds that are most likely located on the edge of the regions of interest are identified.

Some sample results of forming seeds located close to the contours of regions are presented in Figure 2.7

2.5 Seed Growing

This portion of the algorithm is attempting to refine the initial bone mask and create a better partition of the pixels into bone tissue pixels or non bone tissue pixels. The schematic diagram associated with this portion of the algorithm can be seen in Figure 2.8.

As mentioned earlier, because of the differences in bone density and the intrinsic CT imaging artifacts, pixels representing multiple types of tissue are assigned gray level values in the same range. Methods that include local information need to be applied to better delineate objects. Seed growing in the neighborhood of the pixels from the seeded bone mask provides means for bringing the pixels selected as bone closer to the true edge of the bone region. Region growing in the neighborhood of the seeds is accomplished as follows:

Step 1: Identify the $n \times n$ neighborhood of each seed. Experimental testing showed that $n = 9$ is a good choice for this application.

Step 2: Calculate gradient for each seed. For each seed in the seeded bone mask the values of the gradient in the $n \times n$ neighborhood are calculated and the average gradient value is derived.

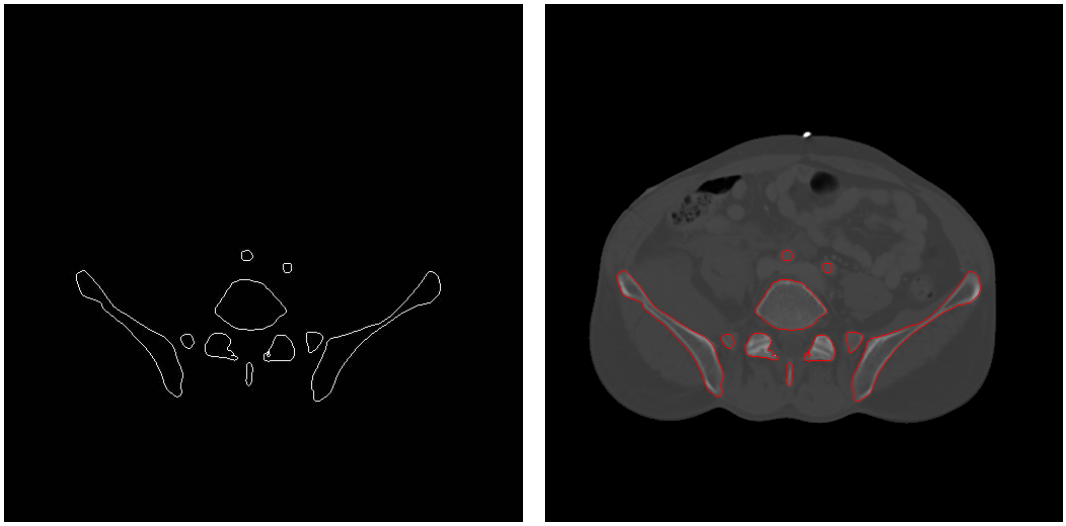

(a) Edge Seeds example A.

(b) Edge Seeds overlapped with the abdominal region example A.

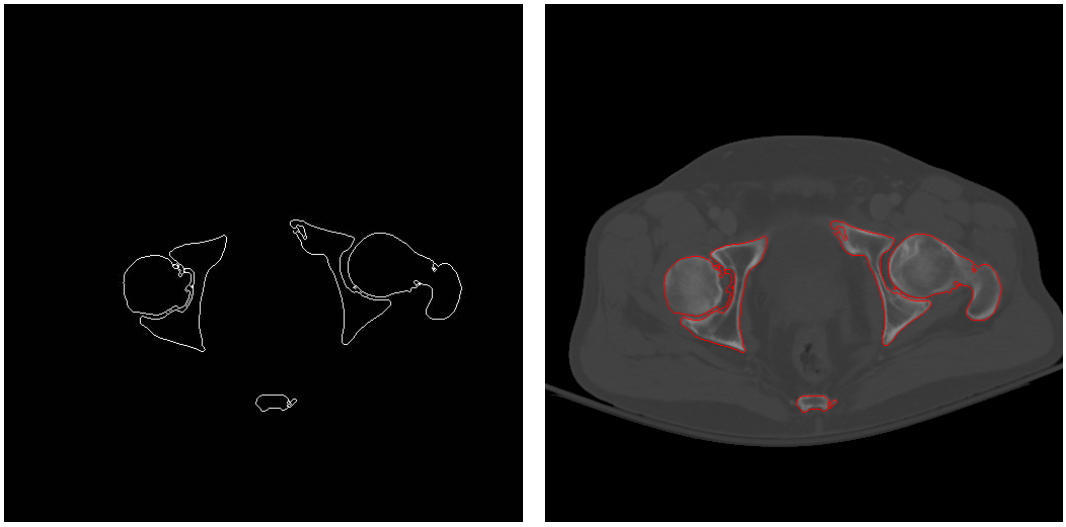

(c) Edge Seeds example B.

(d) Edge Seeds overlapped with the abdominal region example B.

Figure 2.7: Example results for finding seeds close to contours.

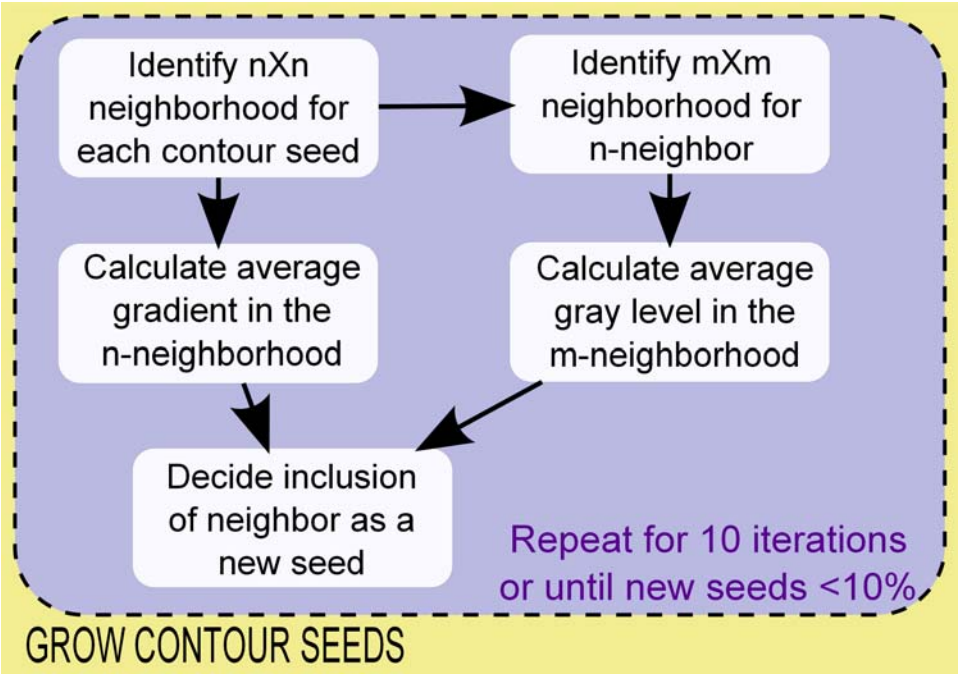

Figure 2.8: Grow Seed Regions.

Step 3: Identify $m \times m$ neighborhood of neighbors. For each of the neighbors in the $n \times n$ neighborhood their $m \times m$ neighborhood is identified. Experimental testing revealed that $m = 5$ is a good choice for this application.

Step 4: Calculate average gray level in the $m \times m$ neighborhood.

Step 5: Decide upon the inclusion of a new pixel in the growing region. A decision on adding a neighbor of a seed to the seeded bone mask is made based on three conditions:

1. The neighbor is located on the inside of the edge
2. The neighbor's gray level value is greater than the average gray level value of the neighbors in the $m \times m$ neighborhood.

3. The gradient value corresponding to the neighbor is higher than the average gradient value.

The steps in the region growing stage are repeated until either 10 iterations have occurred, or the number of new seeds that an iteration adds is less than 10% of the number of existing seeds in the region. Some example results of the region growing can be seen in Figure 2.9. The seed growing process contributes to better connectivity in the segmented regions.

2.6 Summary

This chapter is introducing a method for pre-processing and preliminary bone tissue segmentation from pelvic CT images. Pre-processing of the CT images has the purpose of eliminating artifacts surrounding the pelvic region and is based on morphological operations and blob analysis. Bone tissue segmentation is a hierarchical method that involves a thresholding step in which the threshold is derived from the statistical properties of the gray level values, filtering and seed growing.

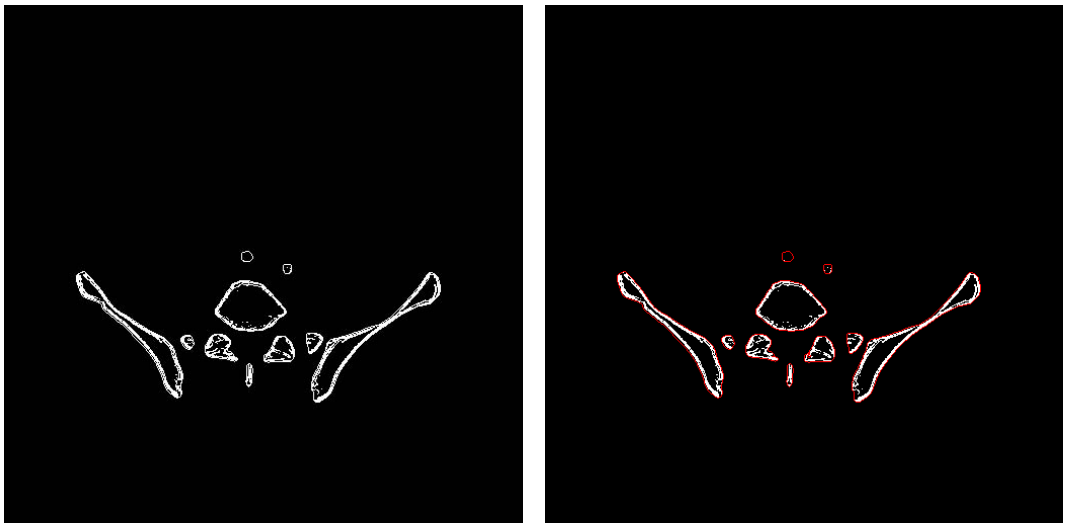

(a) Seed Growing example A.

(b) Edge Seeds and Seed Growing comparison example A.

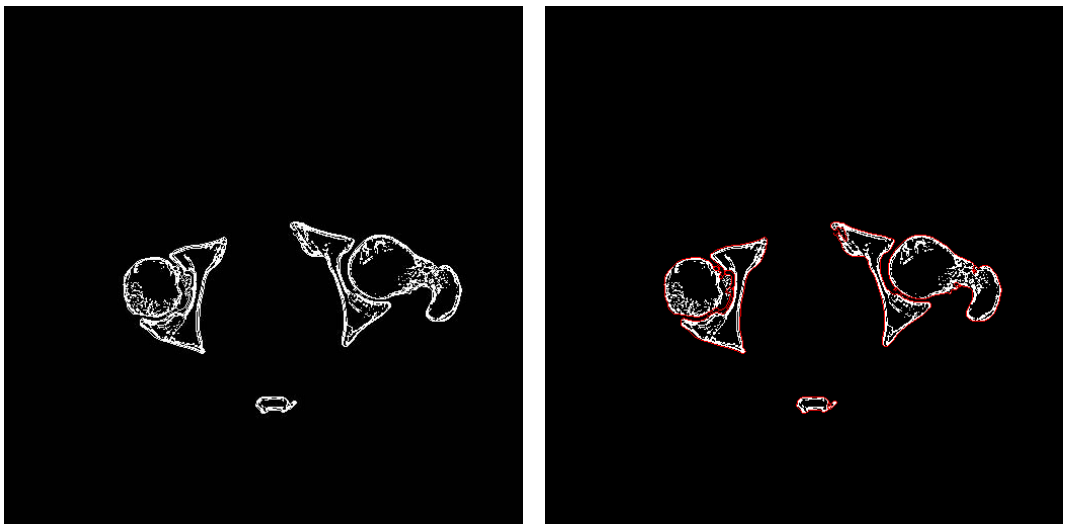

(c) Seed Growing example B.

(d) Edge Seeds and Seed Growing comparison example B.

Figure 2.9: Example results for Seed Growing.

CHAPTER 3 Methods for Shape Matching and Object Recognition

3.1 Overview

Although the information contained in the gray level is vital for distinguishing among regions and labeling them as bone tissue and background, segmentation of pelvic CT images for bone tissue detection cannot rely solely on gray level information. In order to achieve a higher accuracy of CT segmentation, the anatomical and spatial information also need to be included in the segmentation process as other regions might have similar gray level values to bone. A prime example is the case of the overlap of gray level range among bone tissue and fluids, which is typically due to the florescence of iodine enhancer used to detect blood in CT images; an accurate separation between these regions and bone has to be formed not only based on the gray level but also spatial / anatomical details of the regions. This chapter describes the proposed method for distinguishing between bone tissue and regions that, although exhibit the same gray level statistics, are not bone.

3.2 Shape Matching and Object Recognition Method

This section presents the proposed algorithm for shape matching and object recognition. As described in [60], the algorithm starts from individually segmented regions and labels each segmented region as bone or non-bone. An overview of the algorithm is given by Figure 3.1 and each part of the algorithm is further described below.

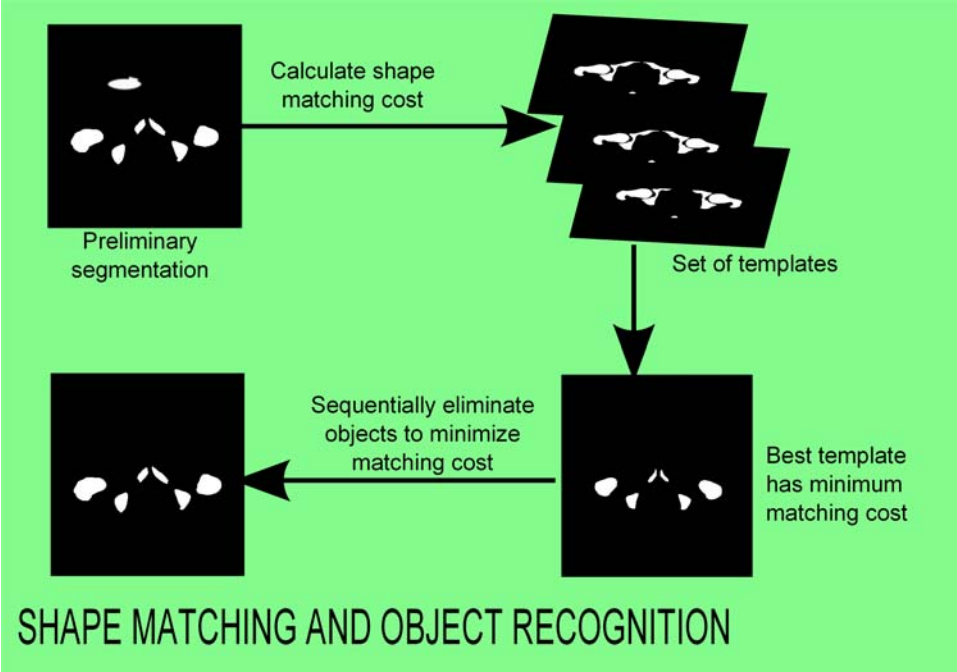

Figure 3.1: Shape Matching and Object Recognition.

3.2.1 Shape Matching

The proposed object recognition method is a modified version of the Matching with Shape Contexts method introduced in [32], [18], [3], [64]. A brief description of the shape matching approach is offered next.

The algorithm starts from two images: the first image is the segmented image and the second image is one of as et of R bone templates. These bone templates were created, through an off-line process, by manual selection of the bone tissue regions. The CT images used to create the bone templates are part of the Visible Human Project dataset. The segmented images, to be matched with the templates, may contain not only bone tissue but also regions that are not present in bone templates.

Each of the two images, i.e. the segmented image and the bone template r, $r \in R$ can have multiple

disconnected components. The steps for the shape matching algorithm are listed below:

Step 1: Automatically select a number of control points in each image. These control points allow the matching between the objects in the template *r*, and the segmented image. The task is accomplished by selecting n_1 control points on the edges of the objects in the segmented image and n_2 control points on the edges of the objects in the template image. The n_1 points on the segmented object and n_2 points on the template *r* object represent percentages of the total number of points on the edges of the objects in each image.

Step 2: Determine shape context. For each point p_i among the n_1 and n_2 control points on the contour of the corresponding objects in the segmented image and template *r*, the " shape context around the point" is defined using a specialized histogram. Specifically, the shape context of the point p_i is described using a histogram $h_{ri}(k)$ of the relative coordinates of the remaining $n_1 - 1$ and $n_2 - 1$ points in the corresponding contours as defined in [3]:

$$h_{ri}(k) = Card\{q \neq p_i | q - p_i \in bin(k)\} \tag{3.1}$$

where $bin(k)$ defines a region encompassed by two rays and two radii, and *Card*. defines the number of members in a set. This histogram defines the shape context of the point p_i.

Step 3: Determine matching cost for individual points. The cost of matching a point p_i [3] in the segmented image with a point q_j in the template image is, as defined by:

$$C_r(p_i, q_j) = \frac{1}{2}\Sigma_{k=1}^{K}\frac{[h_{ri}(k) - h_{rj}(k)]^2}{h_{ri}(k) + h_{rj}(k)} \tag{3.2}$$

where $h_{ri}(k)$ and $h_{rj}(k)$ are the k-bin normalized histograms for the two points. This function determines the matching between any pair of points across the contours of the two objects

and allows quantitative assessment of the fitness of any pairing.

Step 4: Determine matching cost between shapes in the segmented image and the template *r*. The overall cost of a match between the shape in the segmented image and the shape in the template image is the result of minimizing the sum of all individual point cost matches. Since the points on each contour follow a circular order, the matching of points across the two objects can happen only on a finite set of combinations that is limited by the number of points of the counter.

The above steps are repeated for all *r* bone templates. Considering the fact that the segmented CT image can represent a different part of the pelvic region, and that the image often contains some regions that are not bone, as mentioned above, different values of matching will be achieved when the segmented image is matched with different templates. For a given segmented image, even when the right template is selected, one still needs to identify within the segmented image the objects that are bone and the ones that are representing non-bone regions.

The exact choice of the bone template for the segmented slice as well as the exact labeling and separation of the objects in the segmented images associated with one of the bone templates are determined in the next step called object recognition.

Examples of results, comparing the original image and the selected template are presented in Figure 3.2.

3.2.2 Object Recognition

This section focuses on identifying the best matching bone template among the *R* templates and using it to discern among segmented objects, labeling them as bone or not bone. It needs to be

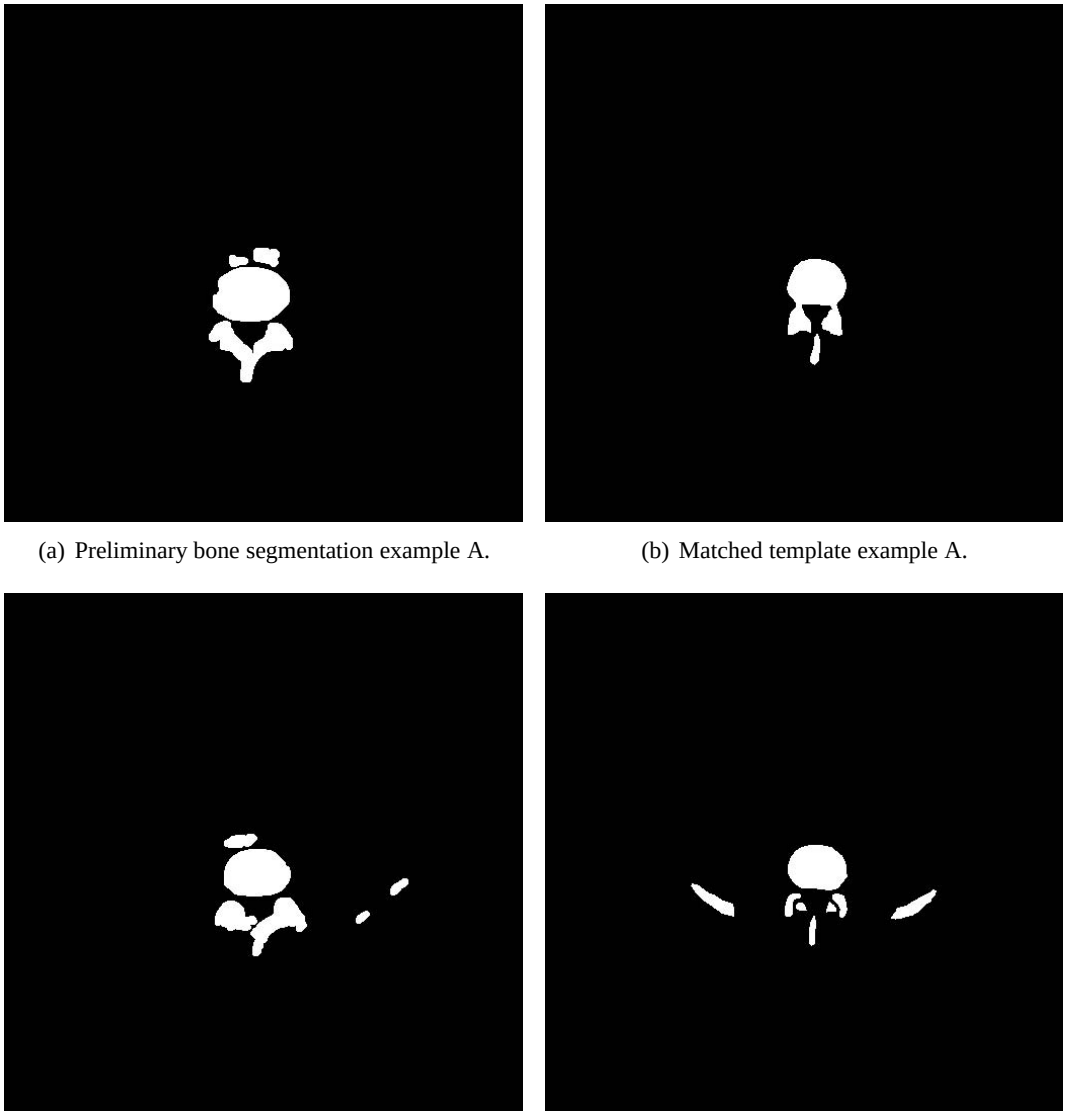

(a) Preliminary bone segmentation example A.

(b) Matched template example A.

(c) Preliminary bone segmentation example B.

(d) Matched template example B.

Figure 3.2: Example results for Template Matching.

mentioned that, using a more detailed set of templates, the algorithm could be extended to discern among bone, hemorrhage, muscle tissue and internal organs.

The steps pertaining to algorithm for object recognition are presented below:

Step 1: Calculate the overall matching cost between the segmented image and all templates in order to find the best matching template r_{opt}, as follows:

$$r_{opt} = arg_{1 \le r \le R}[\min C_r(p_i, q_j)] \tag{3.3}$$

Step 2: Determine separate connected objects in the segmented image.

Step 3: Sequentially eliminate each object from the segmentation and calculate a matching cost between the difference image and the template.

Step 4: Compare the cost of a partition matching with the cost of the original match. This step will exhaustively search and mark the segmented objects within the segmented image that represent bone. If an object representing bone is eliminated the matching between the segmented object and template will increase. Conversely, if the elimination of a segmented object within the segmented image results in a decrease in the matching score, the object is labeled as non-bone. In other words, if the cost is lower than the original matching cost when an object is eliminated, an improvement in the match is obtained and therefore is inferred that the eliminated region was not likely to be a bone region. Also, by eliminating a bone region the segmented image is not as a suitable match to the template as the original image, and therefore the cost of the matching increases.

Step 5: Find a cost of partition matching lower than the cost of the original match. The current

segmentation is initialized with the partition corresponding to the lower cost. Repeat steps 2 through 5. If a lower cost does not exist then stop - the current segmentation is the best match for the template.

The process proposed above labels every region / object within a given segmented image. These objects are labeled as either “bone” or “non-bone”. As motioned above, the algorithm can be extended to include more types of regions such as muscle and fat.

In Figure 3.3 it can be seen that some of the objects that were in the segmentation but have no correspondents in the template were eliminated.

3.3 Summary

The first part of this chapter focuses on describing the implementation of the modified Shape Matching Algorithm as proposed in this work. The algorithm can provide means to calculate a similarity measure between two sets of objects in different images. This method is used to match the segmented image to every one of the available bone templates. Then the object recognition step is described: first the algorithm selects a bone template that best matches the segmented image from the available templates and then all objects within the segmented image are labeled as either bone or non-bone regions. The labeling process is based on the comparison between the values of the new matching costs of the selected template to the alternate versions of the segmentation result. Alternate versions of the segmentation result are generated by sequentially eliminating objects from the original result. The results of implementation of this method for template matching and object recognition for pelvic images are presented in Chapter 7.

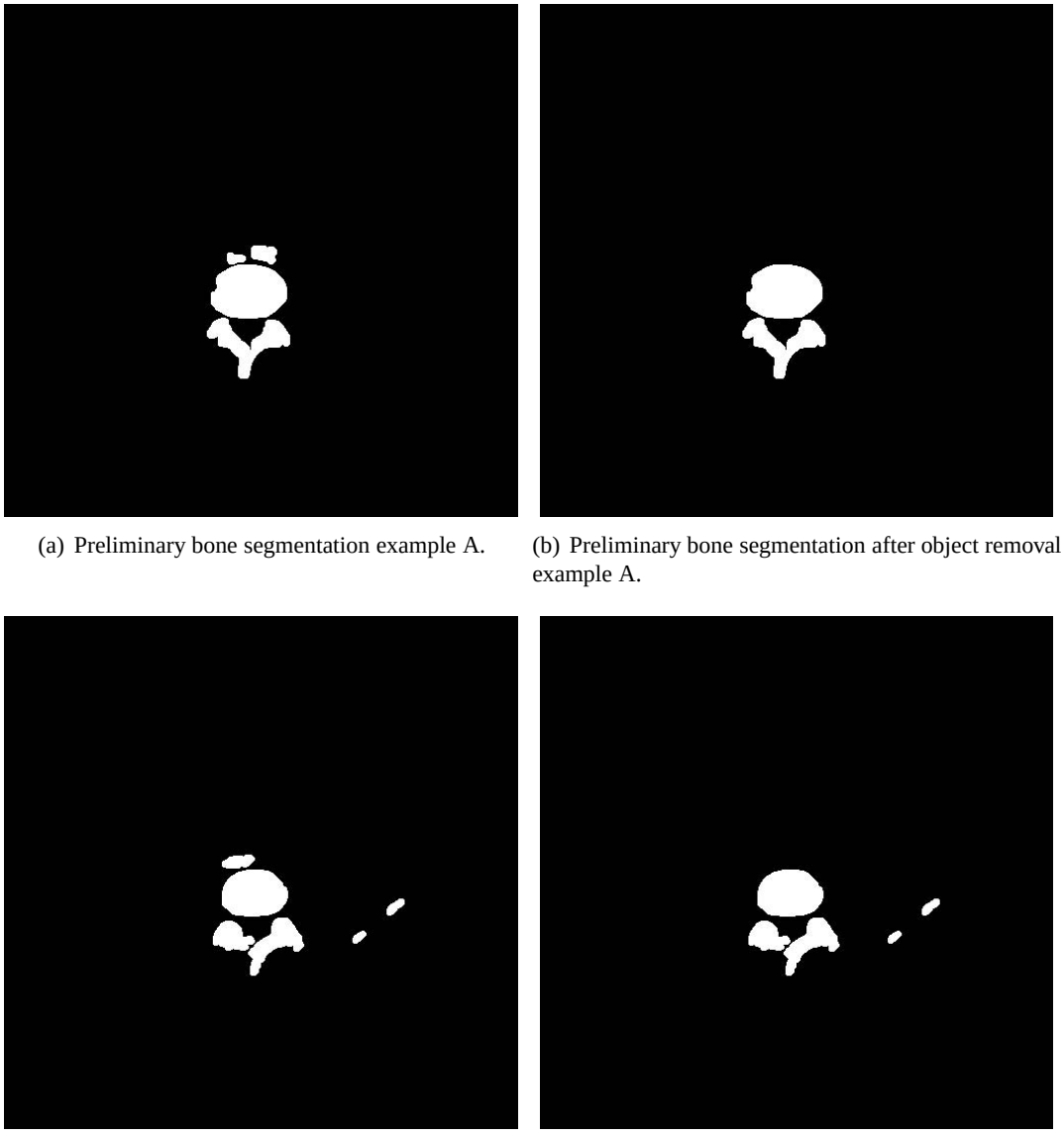

(a) Preliminary bone segmentation example A.

(b) Preliminary bone segmentation after object removal example A.

(c) Preliminary bone segmentation example B.

(d) Preliminary bone segmentation after object removal example B.

Figure 3.3: Example results for Object Recognition.

CHAPTER 4 Methods for Snake Evolution

4.1 Overview

As mentioned in Chapter 1, deformable models, among which Snakes are the most popular family, present several intrinsic advantages. One of the significant advantages is the fact that deformable models directly generate closed curves. In medical image segmentation, when dealing with challenges such as faint edges, non-uniform densities and highly noisy images, deformable models help by producing smoother edges and better connected components. Chapter 2 described the steps needed to perform initial bone tissue segmentation via generation of a set of seed points. However, due to the characteristics of pelvic CT scans, it is very challenging to establish a uniform and sufficient criterion to include all pixels in a bone region. Specifically, the seed generation method provides reasonable initial segmentation results that can characterize the location of the bone, the orientation and the overall shape and size. The edges produced by seed generation segmentation are often noisy and non-inclusive. Nevertheless, the seed generation method presented in Chapter 2 provides the required basis for automatically seeding of a Snake model. The present chapter describes the proposed algorithm for Snake curve initialization as well as the methods of evolving the Snake initial curve. This portion of the work was previously published in [62]. A schematic diagram for Snake initialization and Snake model evolution is presented in Figure 4.1. The elements of this diagram are further described in the following sections.

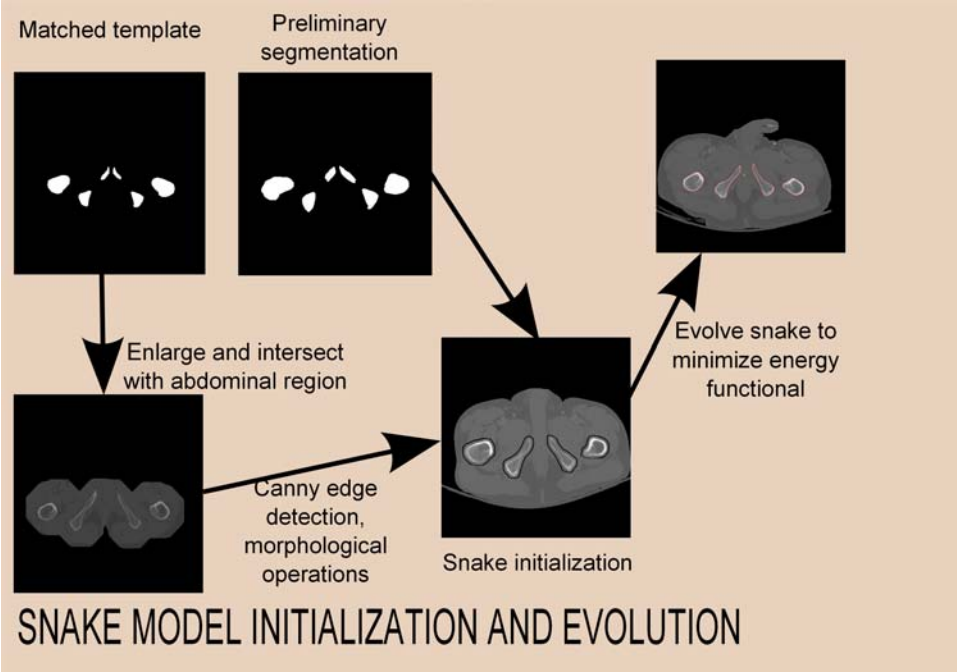

Figure 4.1: Snake model initialization and evolution.

4.2 Snake Model Algorithm

A typical Snake model attempts to minimize an energy functional defined by:

$$E(S) = Int(S) + Ext(S) \tag{4.1}$$

where $S(s)$ defines a parameterized curve / contour defined as:

$$S(s) = (x(s), y(s)) \tag{4.2}$$

where $x(s)$ and $y(s)$ are the parameterized / indexed coordinate functions and s is the parameter / index which lies in the interval of $[0, 1]$. Equation (4.1) introduces two energy functions; the internal energy $Int(S)$, and the external energy $Ext(S)$. The internal energy component represents the total internal deformation energy and is defined as (4.3). The external energy is a force derived

from the image and is often calculated based on the strength of the edges in the image, as discussed later in this chapter.

$$Int(S) = \int_0^1 \frac{\alpha}{2}|S'(s)|^2\,ds + \int_0^1 \frac{\beta}{2}|S''(s)|^2\,ds \tag{4.3}$$

The optimal contour S^* which minimizes the total energy must satisfy the Euler-Lagrange partial differential equation:

$$\frac{-\partial(\alpha\frac{\partial S}{\partial s})}{\partial s} + \frac{\partial^2(\beta\frac{\partial^2 S}{\partial^2 s})}{\partial^2 s} + \kappa\nabla Ext(S(s,t)) = 0 \tag{4.4}$$

For this application, the parameters for Snake model, chosen through experimental testing, are: $\alpha = 1.5, \beta = 0.5$ and $\kappa = 1$.

4.3 Creating Seeds for Snake Initialization

Snake model performance depends on the positioning of the initial curve. The initial curve needs to be placed in proximity of the edge it is attempting to capture as poor positioning might result in the curve being attracted to a false edge, leading to poor segmentation results. Moreover, better and faster results are achieved when the initial curve has a shape similar to that of the object to be segmented. In order to define the initial curve an initial set of seed points is needed. The number of the seeds is another important factor that directly impacts the quality of the initial curve. While relying on a very small number of initial seeds may not yield a good approximation of the shape of the edge, too many seed points not only create noisy edges but also adds to the time-complexity of the algorithm. Another issue regarding the seed points is the way these points are generated / selected. In rather simple applications, where small a number of objects in a small number of images are to be segmented, the seed points are often selected by the human user. However,

in many real-world applications, such as biomedical image processing, where many images are to be processed in a short period of time, manual seed selection is not a feasible option and an automated method of seed selection is much preferred. Specifically, in this application, for a set of CT scan that contains 50 images, manually selecting a set of seeds for every object , in all 50 images, can very rapidly increase the amount of time necessary for image processing. This emphasizes the need to form methods for automated seed selection. In this project, based on the bone segmentation results provided by the seed growing method proposed in Chapter 2 and the shape matching method described in Chapter 3 , an automated seed selection methodology is proposed. This method automatically creates seeds for the Snake model initialization in the following steps:

Step 1: Create a binary version of the segmentation result created by the method described in Chapter 2. Since for seeding only the position of the pixel in the image is needed, no information is lost by eliminating the gray level values.

Step 2: Center and enlarge the template that was selected as the best slice correspondent. Intersect the resulting mask with the image.

Step 3: Perform edge detection in the masked image region. For edge detection the Canny [9] method is used and the threshold parameter was experimentally chosen and set to 0.2. Canny edge detection allows for better connectivity of detected edges compared to other edge detection methods. This effect is primarily due to the hysteresis thresholding that the Canny method uses; strong edges are associated with high gradient amplitudes while faint edges that ensure connectivity between strong edges are also favored.

Step 4: Perform morphological operations to dilate the edges identified using Canny edge and create better connectivity of objects.

Step 5: Perform binary addition between the segmentation result and the enlarged Canny edges. Use the edge of the region formed in this manner to automatically select seeds for Snake initialization.

Step 4: Select a percentage of initial seeds from the edge points. Empirical tests performed on a sample of images revealed that a suitable number of initial seeds would be in the range of 5% to 10% of the number of pixels on the detected edge.

The steps above provide the seeds needed to initialize the Snake according to the formulation described in Section 4.2.

4.4 Snake Evolution

After creating seeds for Snake initialization, the initial curve is defined as:

$$S_0(s) = (x(s), y(s)) \tag{4.5}$$

where $s \in [0, 1]$ and $x(s)$, $y(s)$ are pairs of coordinates for the given seed points.

The initial curve is iteratively deformed under external and internal forces, attempting to minimize the functional:

$$E = \int_0^1 \frac{\alpha}{2}|S'(s)|^2\, ds + \int_0^1 \frac{\beta}{2}|S''(s)|^2\, ds + \int_0^1 \kappa F(S)\, ds \tag{4.6}$$

where $S'(s)$ and $S''(s)$ are the first and second derivatives of S with respect to s, and the weights α, β, κ are the parameters that control the balance among the impact of the tension in the curve,

the rigidity of the curve, and the impact of the external forces on the evolution of the curve, respectively. For a Snake model, the tension and rigidity components are internal energies and have a role in limiting the extent at which the curve expands and bends. External energies are forces that attract the Snake to evolve towards the boundaries it is trying to capture. The external force used in the algorithm is the magnitude of the gradient, as shown below:

$$|\nabla f| = \sqrt{\left(\frac{\partial f}{\partial x}\right)^2 + \left(\frac{\partial f}{\partial y}\right)^2} \tag{4.7}$$

where

$$\nabla f(x,y) = \frac{\partial f(x,y)}{\partial x} i + \frac{\partial f(x,y)}{\partial y} j \tag{4.8}$$

According to the empirical results obtained in the project, at least for pelvic CT segmentation, seed initialization on the outside of the bone contour and contracting to the edges proved to be preferable to initializing of the Snake model on the inside of the bone and expanding the curve towards the edges. This observation matches the intuitive expectation considering the nature of CT images of bone regions: specifically due to the natural variations in bone density across different layers of any given bone, the cortical bone tissue, which forms the edge of the bone, is much brighter than cancellous bone tissue, which forms the core / center of the bone. If the initial seeds are placed inside the gray region closer to the center of the bone, which is formed of cancellous tissue, the Snake captures the inner edge of the bright bone delineation. On the other hand, if the initial seeds are placed inside the bright region, i.e. the cortical bone, the model can easily oscillate between the two edges of the bright cortical region. On the other hand, if the Snake is initialized on the outside of the bone and is evolved to contract inwards, i.e. towards the edge of the bone, there is a much higher likelihood of correctly capturing the outer edge of the bone and therefore segmenting the entire bone region.

In order to insert new data points in the Snake interpolation based on B-splines is used. A linear combination of B-splines is used to represent more complex spline functions, allowing to approximate the edge of the bone.

Given a set of m real valued points, a B-spline interpolation of degree n can be formulated as a linear combination of basis b-splines of degree n, as defined in 4.9.

$$B(t) = \Sigma_{i=0}^{m-n-2} P_i b_{i,n}(t), t \in [t_n, t_{m-n-1}] \tag{4.9}$$

where $B(t) : [t_0, t_{m-1}] \rightarrow \mathbb{R}^2$, $b_{i,n}$ are basis B-splines of degree n and P_is are control points.

The above methodology allows for interpolation in growing the initial Snake curve to generate the final contour of the region and therefore to segment the objects in the image.

Some example results of Snake model initialization and final evolved contour can be seen in Figure 4.2.

4.5 Summary

Chapter 4 introduces a method for automated Snake model initialization and introduces the methodology for evolving the Snake curve. As it will be shown in 7, for the application of pelvic CT segmentation of bone tissue, it was discovered that initializing a Snake model with the initial curve placed on the outside of the bone edge and attracting the curve inwards to capture the edge is more effective than initializing on the inside of the bone and growing the Snake outwards.

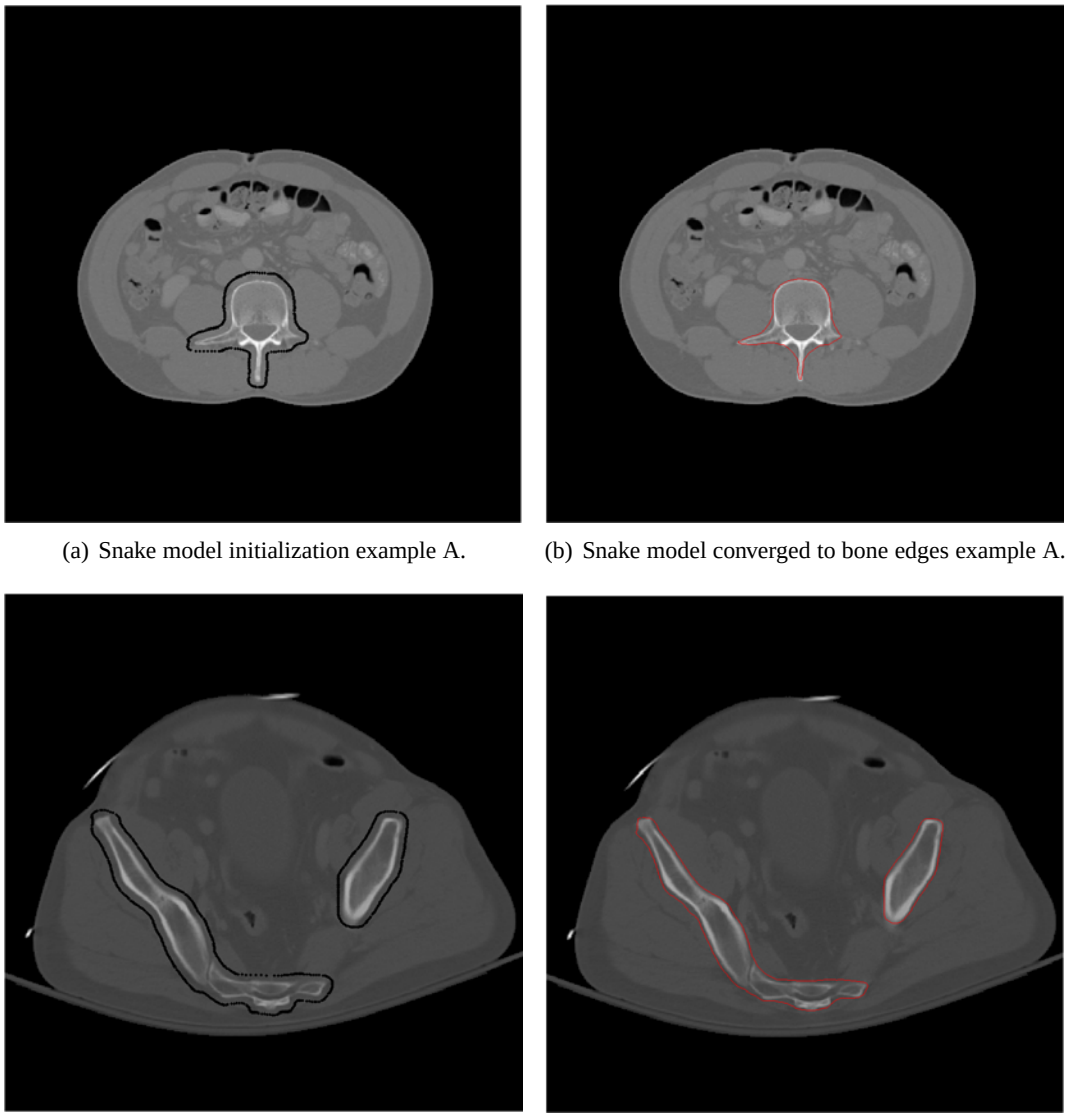

(a) Snake model initialization example A.

(b) Snake model converged to bone edges example A.

(c) Snake model initialization example B.

(d) Snake model converged to bone edges example B.

Figure 4.2: Example results for Snake Model initialization and convergence.

CHAPTER 5 Methods for Feature Extraction

5.1 Overview

Besides detection of bone, in trauma decision making, the detection of the presence of active bleeding, localization of bleeding and quantitative measurement of these hemorrhagic regions are of extreme importance. Spatial and anatomical information needs to be incorporated in the algorithm to allow locating and signaling such regions. Introducing an enhancer to the blood stream is a way of changing the appearance of blood in CT scans and detecting hemorrhage. While enhancers are not always used, the work presented in this dissertation is based on images where an enhancer was used.

In Chapter 3 a method to match a template to the preliminary segmentation is described. Associating a template with a CT slice allows for the more exact identification of the scan segment the CT slice belongs to. Knowing the section of the scan also allows for incorporating the domain knowledge on where hemorrhage is likely to occur.

The present chapter describes the proposed method for the detection of active bleeding. For testing the method, a set of 22 CT images was used, out of which 13 images show cases of active bleeding and the rest do not correspond to bleeding.

5.2 Recognizing Hemorrhagic Regions

In traumatic pelvic injuries, bleeding can occur in several different locations. This dissertation introduces a method for detecting active bleeding in the upper part of the abdomen. In the analyzed dataset, this type of bleeding occurs in the CT slices from the fourth segment of the scan.

The proposed method for detection of hemorrhage consists of the following steps:

Step 1: Identify the width and height of the abdominal region. Based on these measurements, divide the abdominal region into 15 sections, divided into 5 rows and 3 columns of approximately equal size.

Step 2: Identify active bleeding by examining the region of interest. The region of interest was empirically determined to be associated with the box in the second row and third column.

Step 3: Make use of the results of preliminary segmentation to exclude the regions associated with bone from the identified box. This will result in a region of image that contains soft tissue.

Step 4: For the resulting soft tissue image, calculate gray level statistics and a threshold value t_1 by the method described in Chapter 2.

Step 5: Identify the pixel with maximal gray level value in the soft tissue image and create a window of size 50 centered at the pixel location. This step isolates a region which can potentially contain an active hemorrhage region. Such a region would have a mean gray level significantly higher than the overall mean.

Step 6: Calculate gray level statistics and a threshold value t_2 for the $50x50$ pixel window. The

threshold t_2 is established as a summation of the mean of gray level and double of the standard deviation.

Step 7: Make a decision if hemorrhage is present and quantify its size. A decision on the presence of hemorrhage is made by evaluating the condition that the mean gray level of the soft tissue window is higher than the threshold of the soft tissue, t_1.

Step 8: Assess the extent of the hemorrhage by adding the number of pixels having a gray level value higher than t_2.

The measure hemorrhage severity/size is the sum of the pixels detected as hemorrhage, extended by the sum of all the pixels of hemorrhage detected in consecutive slices. This measure offers an estimation of the volume of the hemorrhage.

Example results derived using this method for detecting active hemorrhage are presented in Figure 5.1. Although the size of the testing data set is relatively small, i.e. the dataset contains only 22 images, the results are promising. Work for detecting the presence and assessing the hemorrhage severity is still in progress and a more robust set of measures is expected to be devised and implemented in the future. One objective with regards to the size measure is to form a normalized version of the current measure, where the ratio between the size of the hemorrhagic region to the size of an anatomical feature (e.g. the size of pelvic ring) is calculated. Such a measure would compensate for some calibration issues encountered when dealing with different CT machines or using the same machine at different settings.

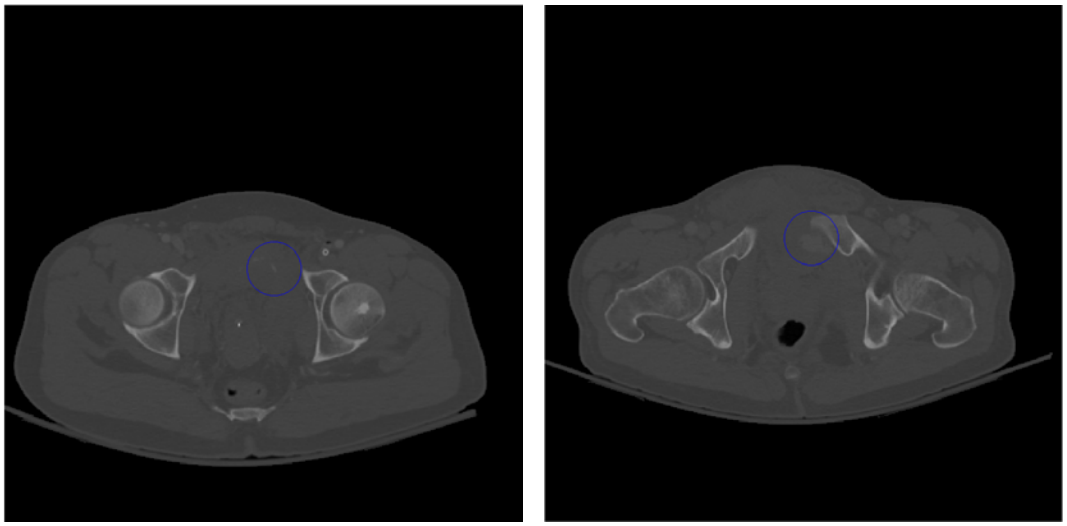

(a) Active hemorrhage example A. (b) Active hemorrhage example B.

Figure 5.1: Example results for hemorrhage detection.

5.3 Summary

The present chapter describes the proposed method for detecting regions of active hemorrhage. Determining whether or not a segmented image contains a hemorrhagic region is a challenging task and anatomical knowledge needs to be incorporated in the algorithm in order to perform this task. The automated detection of hemorrhage also allows for the quantitative assessment hemorrhage severity.

CHAPTER 6 Generating Rules for Outcome Prediction

6.1 Overview

In the trauma care environment, a large amount of information needs to be processed in a short amount of time in order to form a decision regarding diagnostic and/or treatment planning. As a result, there is an increased need for computer-aided decision making systems. Such systems have to provide reliable recommendations, preferably in the form of prediction rules, that allow the caregivers to understand and monitor the reasoning behind such recommendations. The present chapter is dedicated to rule generation that is part of this project. A schematic diagram of this part of the algorithm is presented in Figure 6.1.

6.2 Dataset

The dataset used in this section is provided by Carolinas Healthcare System and comprises of 45 pelvic trauma cases which is a relatively small number but some were sent to ICU while others with less serious injuries were sent home or a hospital ward. In all cases, patients survived the injuries. The dataset has a reasonable distribution in terms of outcome, the two classes having approximately the same number of members: 20 are sent to ICU and 25 are dismissed home or to a hospital ward. Demographic and injury scores, extracted from patient medical records, include: age, gender, Injury Severity Score (ISS), Glasgow Comma Score (GCS) and mechanism of injury (e.g. fall, motor-vehicle). The dataset was formed such that for all cases X-ray and CT scans taken on the admission date were available.

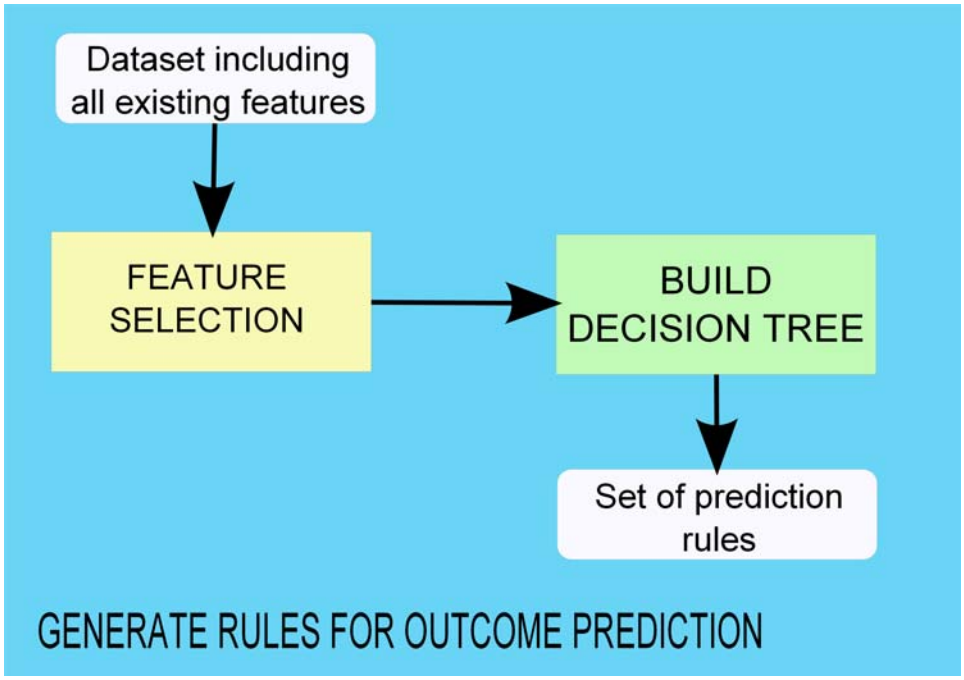

Figure 6.1: Outcome prediction rule generation.

6.3 Grammatical rule generation

Features extracted from CT images are combined with the features extracted from X-ray, which are generated by a companion project, and injury scores such as Glasgow Coma Score (GCS), Injury Severity Score (ISS), together with injury mechanism and demographic data, to form the dataset. The Weka software was used to perform attribute selection and to build the decision trees. In order to choose features relevant for the prediction, the correlation based feature subset evaluation is used [15]. The method evaluates each feature subset based on the degree of redundancy among them as well as the individual predictive power of each feature. This method favors subsets of features having low correlation within the subset and high level of correlation with the class label. Using this method of feature selection, the subset of features that was found to be most relevant contains Injury Severity Score (ISS), Glasgow Coma Score (GCS) and presence of pubis fracture.

The dataset formed by the values of features in the selected subset was then used as the input to the C4.5 [40] and CART [7] algorithms. Both algorithms are well established in the machine learning community as effective tools to derive decision trees. Both decision trees algorithms extracted similar patterns from the data which indicates the patterns extracted from the data were consistent and not associated with the choice of algorithm used. The tree generated by C4.5 is presented in Figure 6.2. As it can be seen, the algorithm places the presence of pubis fracture high in the tree. Such a finding reinforces the fact that extracting features from medical images is important in the development of a method for assisted decision making. Results were generated using 10-fold cross validation in the case of both decision tree algorithms.

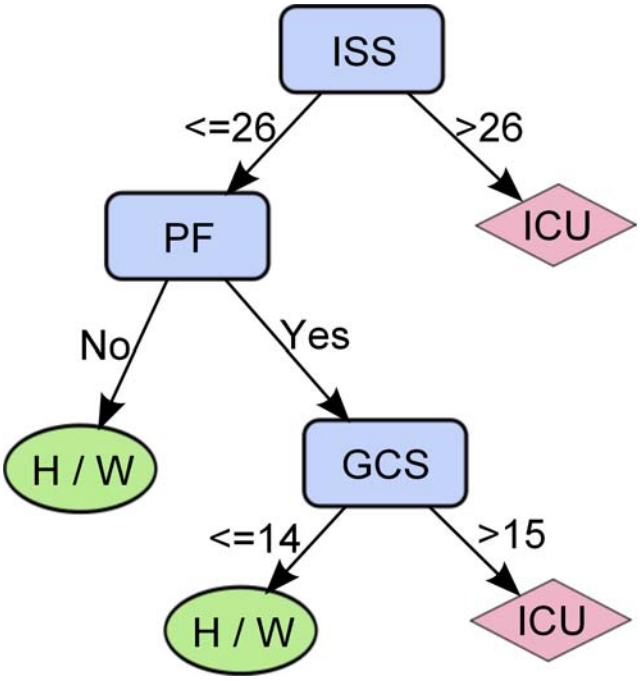

Figure 6.2: Decision tree derived by C4.5.

ISS - Injury Severity Score, GCS - Glasgow Coma Score, PF - Pubis Fracture, H/W - Home or hospital ward, ICU - Intensive Care Unit.

A statistical assessment of the results is presented in Table 6.1, which indicates promising results

Table 6.1: Results of C4.5 and CART classification.

	C4.5	CART
Sensitivity	84.0%	84.0%
Specificity	70.0%	60.0%
Accuracy	77.8%	73.3%

and the expectation that the performance of the algorithm may be improved by using a larger dataset and more balanced classes.

As previously mentioned, the dataset used to derive the rules in this section was relatively small. However, the fact that, when the dataset was processed using CART and C4.5, features extracted from images were placed very high in the generated decision trees suggests that such features are of importance in establishing a diagnosis. More extensive testing on a larger data set and more features need to be included such that the derived rules can be used in clinical setting. Also an extensive testing process, in collaboration with physicians, needs to be conducted towards validating such rules.

6.4 Summary

The present chapter describes methods for assessing the severity and outcome of traumatic pelvic injury in terms of predicting whether the patient will be sent to the Intensive Care Unit (ICU) or dismissed to a hospital ward or home. Predictions on such outcome are formed based on decision rules extracted from decision trees. The initial set of features considered for decision making includes demographic and physiological information, as well as features extracted from analyzing X-ray and CT images. The derived sets of rules are similar for the two decision trees algorithms

that were used - C4.5 and CART. Results are promising and the generated rules exhibit reasonable predictive power, with relatively high accuracy, sensitivity and specificity. Only a small number of features were evaluated as having predictive power, these features include features extracted from images.

CHAPTER 7 Results and Discussion

7.1 Overview

This chapter presents the results of the proposed methodology and briefly discusses the results. Several categories of results are presented, which correspond to different steps of the proposed method. In each category the results created based on multiple samples will be provided. These samples represent different slices of the CT scans taken from different patients. For generating the results presented in this dissertation a data set consisting of 684 CT slices from eleven patients each having between 45 and 75 different CT images was formed. The images for each patient were selected to represent a variety of anatomical structures within a pelvic CT scan and display similar structures within the group of patients. The variations among these samples allow better assessment of the system performance when dealing with different shapes of bone and different patients.

7.2 Results

Results corresponding to different stages of the proposed methodology are presented in separate sections, as follows.

7.2.1 Eliminating surrounding artifacts and extracting the pelvic region

The results presented in Figure 7.1 demonstrate how successful the proposed pre-processing method is in eliminating the surrounding artifacts such as the CT table and cabling that is visible in most of the CT images. Additional results are presented in 2.3. This step is important

because inclusion of artifacts can influence gray level statistics and create complications in the future steps of the algorithm. Results of artifact removal were evaluated visually and by calculating the percentage of the removed area compared to the total area of objects in the raw image. On the testing dataset mean area removed from each image is approximately 6%. However, the percentage of removed area also depends on the type of artifacts present in each scan; one of the tested scans, in which patient extremities were present the average removed area was 18%.

Looking at the right column of images, in Figures 1(b) and 1(d), it can be noticed that the cabling and other background objects were eliminated compared to the corresponding original images presented in the left column, in Figures 1(a) and 1(c) respectively. In all the tested images the method successfully removes the artifacts surrounding the abdominal regions although there are images, such as Figure 1(d), in which the upper part of the CT table is not completely removed.

7.2.2 Initial mask formation

Initial mask formation, as shown in Figure 7.2, creates an initial frame for formation of the seeds. As discussed in Chapter 2, although gray level thresholding is capable of accurately locating bone regions based on their gray level values, it also selects other regions that are above the threshold. To alleviate this problem a solution is designed in which an intersection between the thresholded initial mask and an enlarged template corresponding to the examined CT slice is formed. In most examples tested, erroneous inclusion of regions based on the initial gray level thresholding usually occurs in the first segment of the CT scan, roughly in the first fifth of the scan, such as in the examples provided in Figure 7.2. Although initially intersection of results and enlarged template was used uniformly throughout the processing of the scan, currently this method is applied only

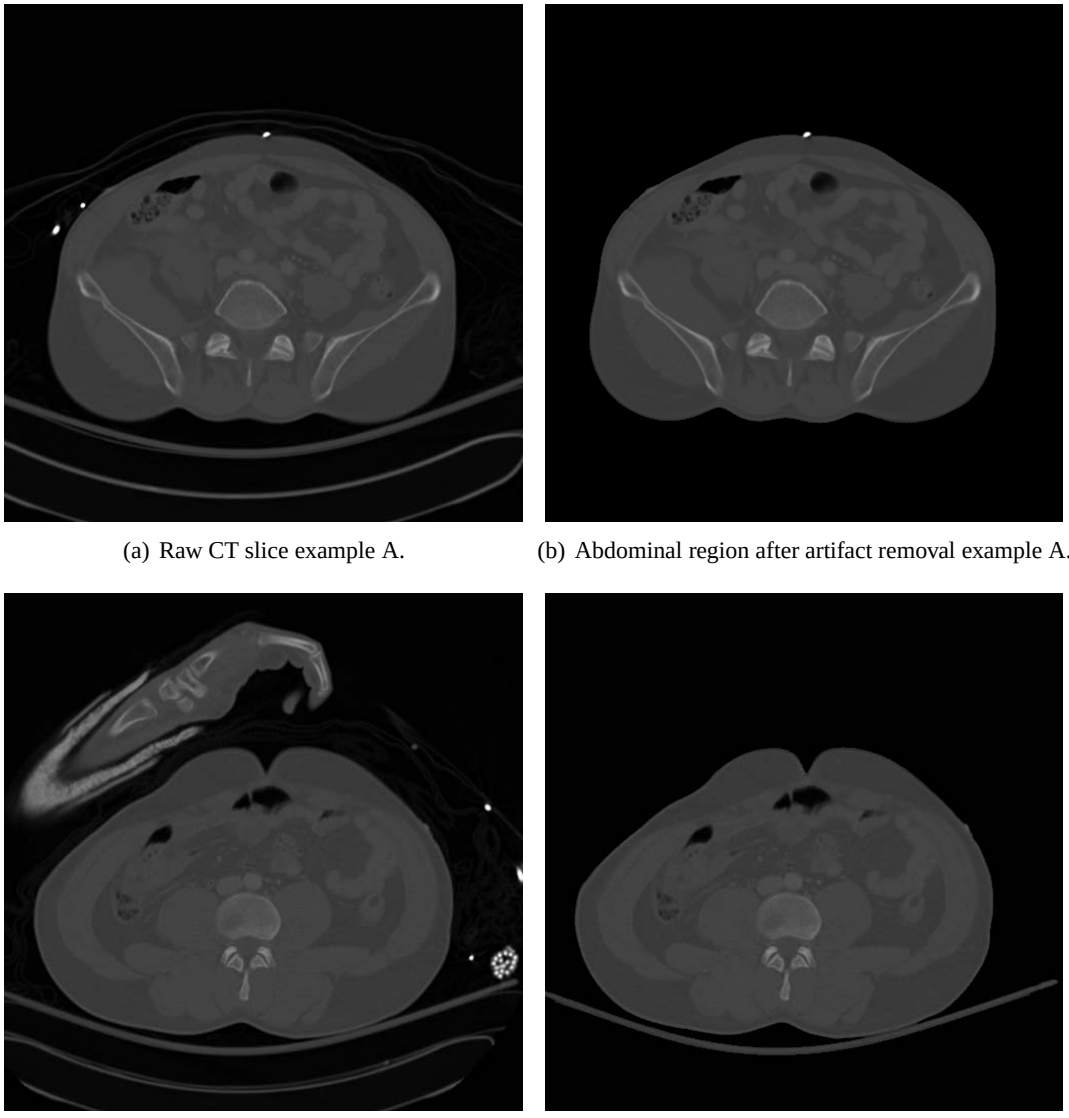

(a) Raw CT slice example A.

(b) Abdominal region after artifact removal example A.

(c) Raw CT slice example B.

(d) Abdominal region after artifact removal example B.

Figure 7.1: Sample results for extracting the pelvic region from the raw CT Image.

to segments of the scan which consistently prove to exhibit this problem. In the testing dataset, formation of initial mask via thresholding was evaluated to have reasonable overall performance by forming effective initial segmentation of bone. However, approximately 22% of the examined segmentation results could benefit from applying the method which intersects an enlarged template with the result of the thresholding. Most of the slices that constitute this 22% are located in the upper portion of a scan, each segment representing the first one fifth of the total number of slices in the scan. Based on this evaluation, the method was adjusted such that only slices located in the first segment of the scan make use of the method.

It can be noticed in Figure 7.2 that thresholding based on statistical properties of the gray level, combined with filtering of the image yields a relatively accurate representation of the bone tissue. The thresholding method was preferred for creating the initial segmentation due to ease in implementation of the thresholding algorithm, low computational complexity and quality of results. However, by examining the results it can be observed that the connectivity of the bone regions needs improvement. The next steps of the algorithm attempt to address these issues. Visual inspection of the results indicate reasonable performance of the method. Results of the initial mask formation, after intersection with the enlarged template, were assessed visually. In the testing dataset approximately 7.1% of the initial segmentations were deemed to be of insufficient quality, which would affect the results of other steps in those slices.

7.2.3 Seeded mask formation

Examples of results produced by the method described in sections 2.4 and 2.5 are shown in Figure 7.3. These results will be used in shape matching and to derive the location of the seeds to be used for initialization of the Snake model.

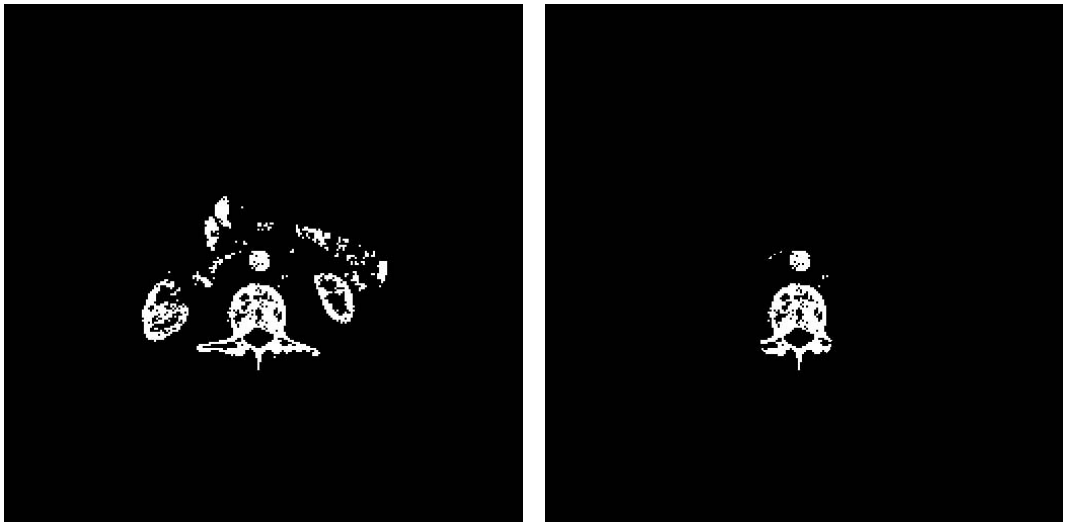

(a) Initial thresholded mask example A.

(b) Initial mask intersected with the enlarged template example A.

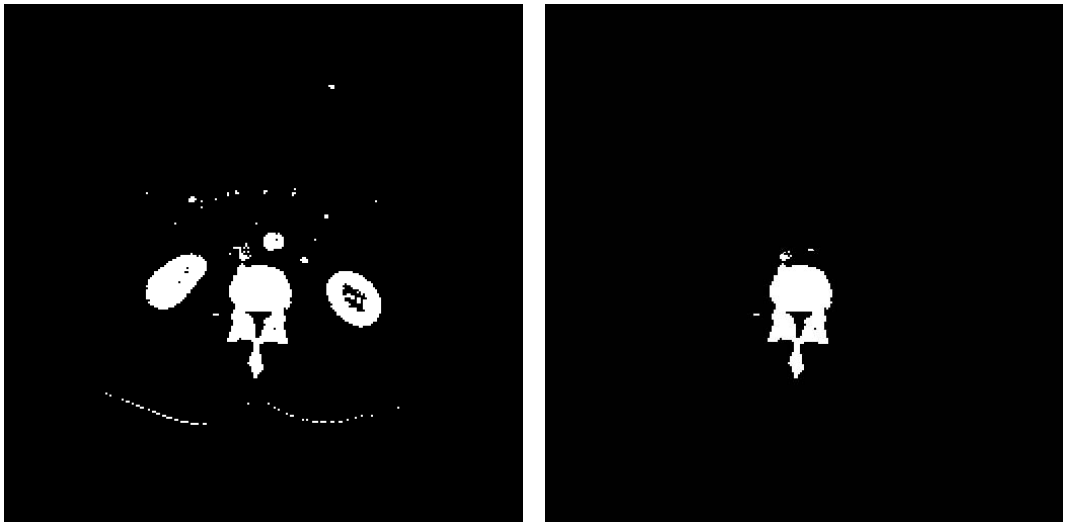

(c) Initial thresholded mask example B.

(d) Initial mask intersected with the enlarged template example B.

Figure 7.2: Sample for thresholding and Initial Mask formation.

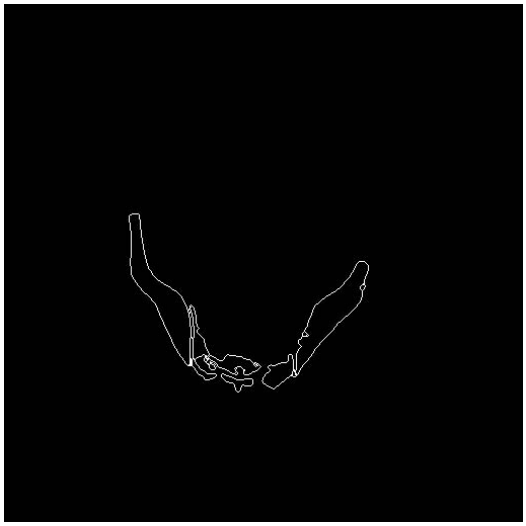

(a) Contour seeds example A.

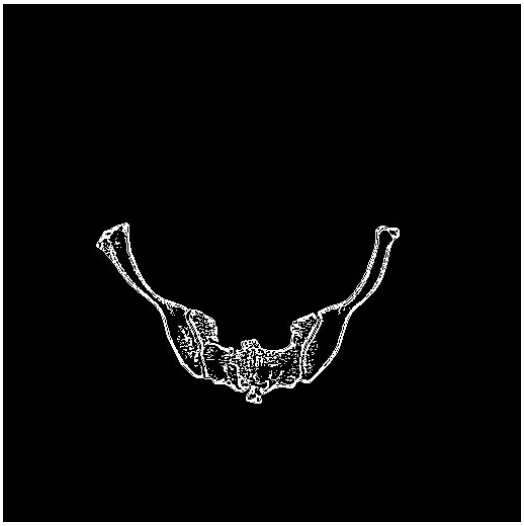

(b) Comparative results of region after growing example A.

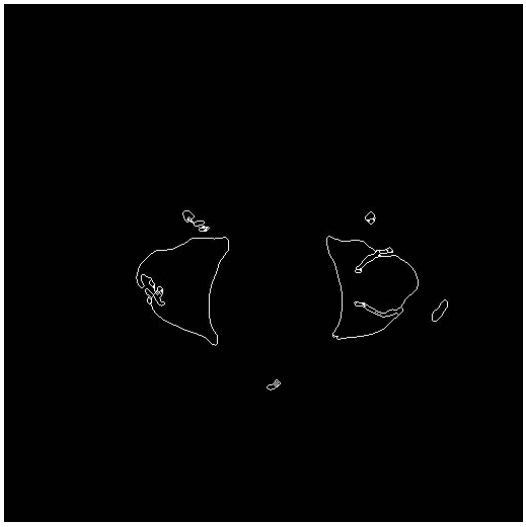

(c) Contour seeds example B.

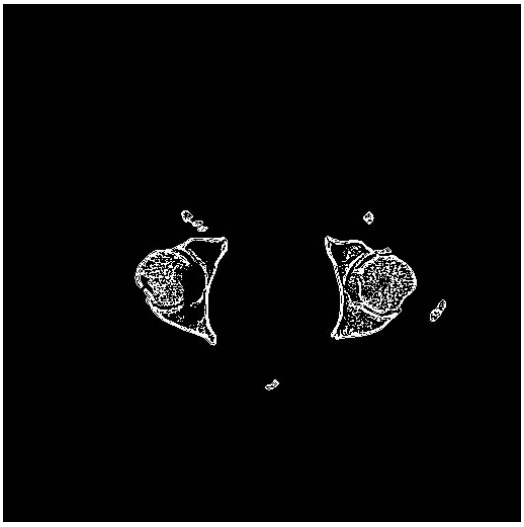

(d) Comparative results of region after growing example B.

Figure 7.3: Sample Seeded Mask Results. Contour seeds compared to seed growing result.

This seed growing step further improves the connectivity of the bone tissue. Region growing is performed under very constrained conditions and only allows for adding seeds located inside the region delineated by the edge seeds. Such assumption prevents the region growing process from spreading into non-bone surrounding areas. In addition, it helps with detecting bone edges that were not initially detected. For instance, note that in Figure 3(d) the edge of the bone on the left hand side of the image are captured although the edge is not captured by the initial seeds.

The union of the seeds on the contour and the seeds added through seeds growing creates a delineation of bone which can be used to match the current examined slice to a template that is most suitable as described in Chapter 3. The ability to determine the approximate location of the slice in the scan is extremely important as it can help deploy specialized methods for each section of the scan. The preliminary segmentation is created based on the results of the seed growing method, and the results of preliminary segmentation were assessed visually. The evaluation criteria were for the segmentation to locate all bone regions, not show an excessive amount of non-bone regions and display reasonable connectivity of segmented bone. Given these criteria, approximately 13.54% of the 684 testing slices were found to display poor preliminary segmentation.

7.2.4 Matching a template to the analyzed slice

In this section, results produced by the shape matching algorithm are presented. Shape matching is used to associate a template with the slice being examined. The association is made by selecting the template which has minimal matching cost to the preliminary segmentation. Segmentation is formed based on the binary addition of the contour seeds and seeded region after seed growing. Choosing the template with minimum matching cost proves to be a simple and efficient technique for creating an accurate association but the criteria being used for the selection may be modified

in future work. Sample results for template matching using the shape matching method, presented in Chapter 3, can be seen in Figure 7.4. The shape matching method proved to be robust in choosing suitable templates. Evaluation of the results of shape matching suggests that only 3.8% of the tested templates were not matched with a suitable template.

7.2.5 Sequential elimination of non-bone objects

Some of the results of the proposed method for excluding non-bone objects, which was discussed in Chapter 3, are presented in Figure 7.5.

As it can be seen in Figure 7.5, the sequential elimination based on the Shape Match method can successfully identify the regions that do not match the template and successfully eliminates the majority of objects that do not match the template. The sequential elimination method successfully removed non-bone regions from majority of the problematic preliminary segmentations; only in 6.8% of the total number of slices the non-bone regions were not correctly removed.

7.2.6 Snake modeling

Sample results of the Snake modeling, starting from automatically generated seeds are presented in Figure 7.6. The external force used in this study was the magnitude of the gradient of the Canny edge processed image. Snake initialization is done in automated manner and is based on the results obtained by the preliminary segmentation and template matching. Each Snake model in one image is constrained to evolve inside a mask that captures the desired object. This approach proved to alleviate some of the problems concerning the convergence of the Snake model to edges of surrounding objects. The initial placement of the curve and initial contour shape reflect on the performance of the Snake model and drive it to better converge towards concave edges. For the snake model method results suggest that initialization is successful in 64.42% of the cases. Results

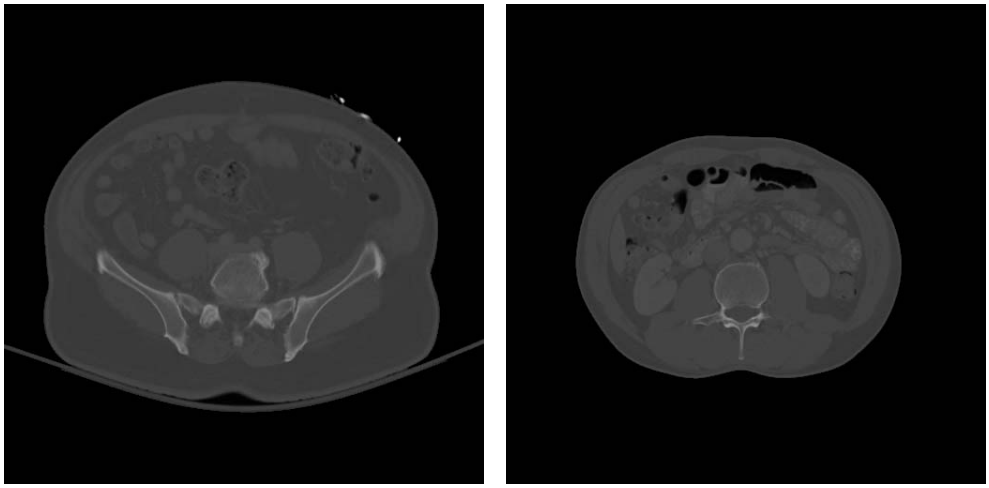

(a) Abdominal region example A. (b) Abdominal region example B.

(c) Preliminary segmentation example A. (d) Preliminary segmentation example B.

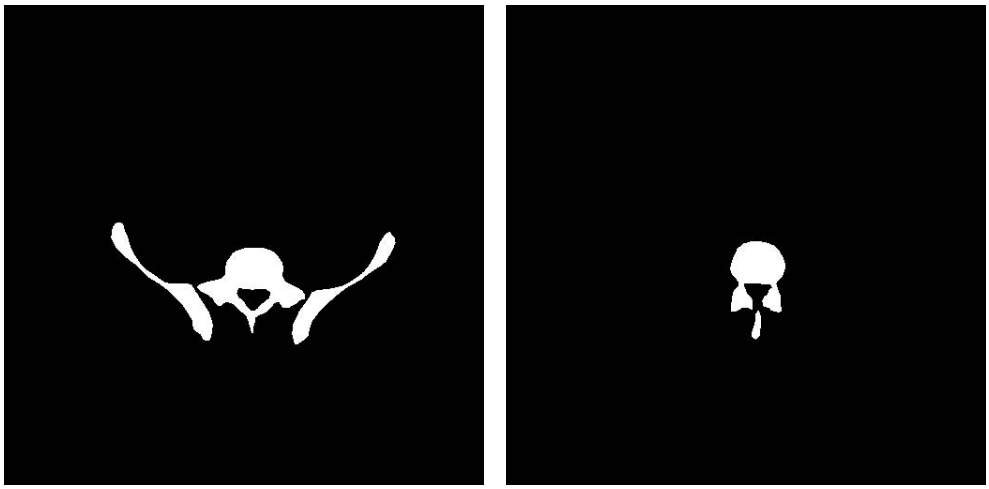

(e) Selected template example A. (f) Selected template example B.

Figure 7.4: Sample Results for template selection using the Shape Matching method.

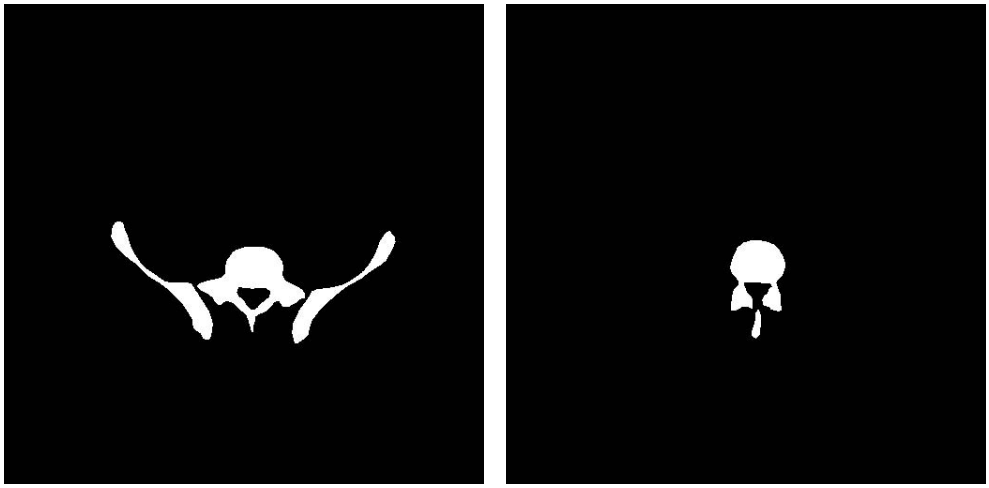

(a) Selected template example A.

(b) Selected template example B.

(c) Preliminary segmentation example A.

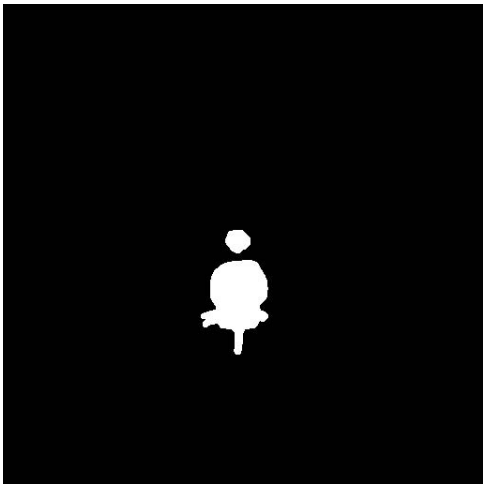

(d) Preliminary segmentation example B.

(e) Segmentation after sequential elimination example A.

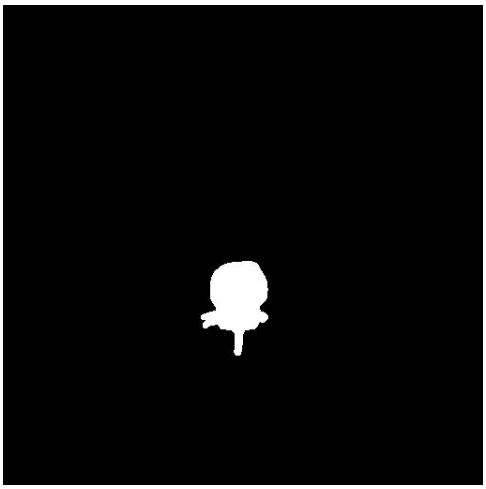

(f) Segmentation after sequential elimination example B.

Figure 7.5: Sequential elimination of non-bone objects from segmentation.

of snake convergence in cases of successful initialization show that the snake curve converges in 96.8% of the cases.

7.2.7 Feature extraction

Results of bone segmentation and template matching create the grounds for analyzing the CT slices in a organized and specialized manner, mimicking the approach taken by experts. Specialized methods can allow search of specific injury patterns in the examined slice. The work presented in this dissertation proposes methodologies for active bleeding detection and assessment of hemorrhage severity. Although the dataset available for testing is relatively small, the results appear to be promising.

7.2.8 Rule generation

Although the results obtained by the classification method are formed using a relatively small dataset, they confirm the fact that extracting features from medical images is important in creating a computer-assisted decision making system. Two well established machine learning methods, CART and C4.5, were used to form decision trees from the dataset and both retrieve similar rules, which suggests that the pattern are real. These rules were presented in 6.

7.3 Discussion

The main observations regarding the results of the proposed methods are:

- The designed sequence of morphological operations combined with performing blob analysis form a successful method of eliminating the majority of surrounding artifacts and extracting the pelvic region.

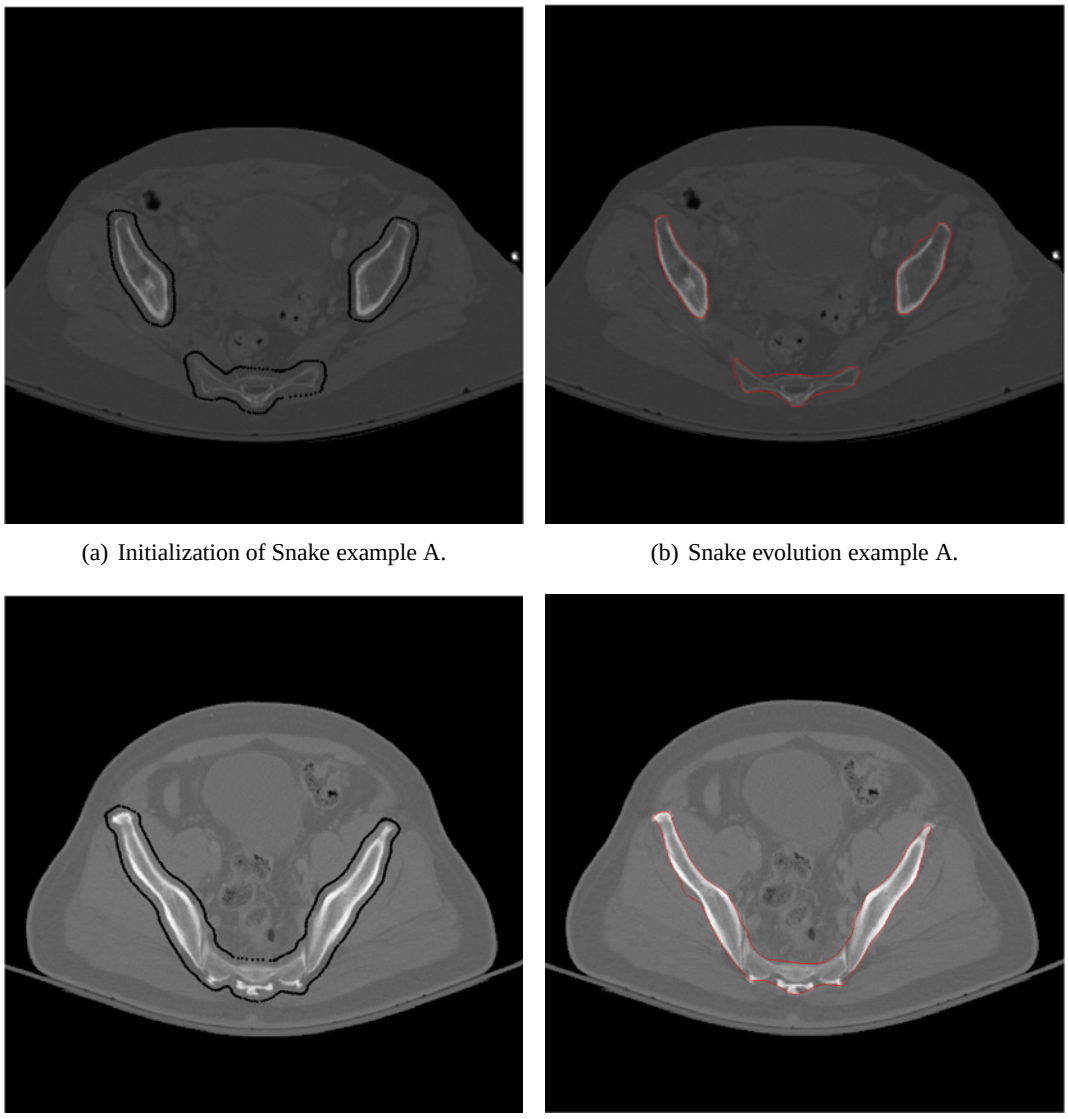

(a) Initialization of Snake example A.

(b) Snake evolution example A.

(c) Initialization of Snake example B.

(d) Snake evolution example B.

Figure 7.6: Sample results of Snake Modeling for the segmentation of bone.

- Filtering of the image and thresholding it using a threshold derived form the statistical properties of the gray level in the pelvic region performs well in providing an initial segmentation of bone.

- The development of a suitable method for determination of threshold is vital for the segmentation performance as significant amount of gray level variations exists among different CT images and a threshold that is universally valid for all CT images cannot be easily established.

- The method for automated seed generation is vital for this application and helps in reducing the processing time by eliminating the need for manual interaction with the system.

- Region growing under restrictive conditions improves the connectivity of the segmented regions while it avoids incorporating numerous false pixels in the segmented regions.

- The Snake model designed in this dissertation improves edge smoothness and connectivity in lateral pelvic bones. Automated initialization, which places the seeds close to the edge of the bone and forms an initial contour of similar shape to the bone, ensures reasonable convergence of the model.

- Initial seeding on the exterior of the bone is preferred for the Snake model, compared to seeding in the inside of the bone as suggested in the literature. Results prove that the model can more accurately converge to the bone edges when seeds are placed on the outside of the bone.

- The association between the examined slice and a template, which is based on shape match-

ing, further improves the segmentation result by allowing deployment of specialized methods that address problems commonly encountered in the slice, such as bone connectivity and density.

- The shape matching and object recognition methods are robust in recognizing bone and non-bone objects. Even small differences in the segmentation result are detected as changes in the matching cost with the template. This conclusion was reached by performing sequential elimination of segmented objects and comparing the new costs of matching to the template with the original matching cost.

CHAPTER 8 Conclusion and Future Work

8.1 Overview

Traumatic injuries are the main cause of death for people 40 years and younger, and as such, serious health risks for the general population. Traumatic pelvic injuries and associated complications, such as blood clots traveling to the brain or lungs and resulting complications due to infection, have a significant impact on the mortality rate of the above-mentioned age group.

Examining pelvic CT images is one of the main tools for establishing an accurate diagnostic for patients suffering from traumatic pelvic injuries. There is a large number of pelvic CT images that need to be closely examined by experts in order to form a diagnostic. Introducing a computer-aided decision making system that can automatically examine medical images and offer recommendations to physicians could help improve the accuracy of the decision, reduce both the decision making time and the cost of healthcare.

This dissertation introduced methods that can help resolve some of the challenges that come from automatically examining CT images. This chapter provides a review of the main conclusions drawn from the methodologies and results described in this dissertation. It also explains the future work, ideas, and steps to be pursued by this project in order to further explore the formation of a computer-assisted traumatic pelvic injury decision making system.

8.2 Conclusions

Segmentation of CT pelvic images is a vital initial step for extracting image features and ultimately creating an automated system to assist experts with diagnostic decisions on traumatic pelvic injuries. In order to address this need:

- A method for automated selection of initial seeds for region growing and deformable models algorithms was introduced. This method reduces the time of CT image processing compared to manual seed selection. The method also eliminates the need for manual interaction with the system in order to select the seeds.

- As another improvement to the existing segmentation methods, shape matching is utilized to help in discerning which objects are bone regions and which are not. The use of shape matching improves the specificity of the algorithm and its ability to distinguish bone structures from regions of that are not bone but have similar gray level statistics. Template selection based on shape matching has a significant impact on improving accuracy of the results. Template matching allows for cross referencing between successive slices and identifying the section of the scan that is currently examined. Having the knowledge of which section of the scan the slice belongs to can help in deploying specific computational methods that address specific challenges. Template matching is an effective approach for incorporating anatomical knowledge into the algorithm and can be extended to help in the segmentation of other structures such as organs and muscle.

- A Snake model approach was designed to capture some of the features of bones, such as edge continuity, and improve connectivity of segmentation. The main reason for segmen-

tation of pelvic CT Images being a challenging task is the large amount of variation in the anatomical characteristics of the objects in CT images such as the shape and placement of different bones in different slices of CT. Depending on the geometric features of the bones, including the anatomical information in developing the Snakes method can aid to the correct segmentation of bones. However, limitations of Snakes, such as their poor convergence to concave boundaries, result in a poor segmentation in case of more intricate shapes. The Snake model developed in this dissertation proved to perform successfully on a variety of CT slices and bone shapes.

- A methodology was proposed that combines all patient data, including features extracted from CT images, to form grammatical rules on severity and outcome of pelvic injuries.

8.3 Future Work

Future work includes the following items:

1. To improve the results of segmentation and reduce average image processing time. Currently, the average processing time for one image is under a minute. However, translating the algorithm into a different programming language can significantly reduce the processing time.

2. To explore other approaches in template matching and extend the set of templates. Currently the template set includes one hundred templates that were formed using manual segmentation of CT images from the Visible Human Project dataset. There are several approaches to template matching that may have a positive impact on the algorithm:

(a) Extending the set of templates. By introducing more templates to compare to, some challenges associated with variability across bone shape, size and relative location may be addressed.

(b) Finding a suitable scaling factor for templates. By examining the size relationship between preliminary segmentation and the matched template, the matched template size can be adaptively modified to better capture the size of the bone in the examined slice.

(c) Labeling the set of templates to exhibit the similarities in the structure. By labeling the set of templates the results of cross referencing between successive slices can be improved.

(d) Exploring methodologies to center the template. By positioning the template so that it is aligned with the bone structures to be segmented, a better overlap between the template mask and the bone can be achieved.

(e) Exploring possibilities of positioning, scaling and rotating of individual objects in the templates. By performing such adjustments using affine transform, some of the challenges due to the bones being positioned at different distances and having different orientations can be addressed.

(f) Extending template matching to capture other structures. Being able to extend template matching to help with the segmentation of organs and muscle can influence the template matching of bone.

3. To process the segmented images to more accurately detect the existence, location, and severity of fractures. It is also important to identify diagnostically important types of fea-

tures to be used for diagnostic rule.

4. To detect regions of inactive bleeding, and to assess the severity of hemorrhage by estimating the volume of accumulated blood.

5. To correlate the above information to help with diagnosis. Ultimately, features extracted from fracture detection and hemorrhage severity must be correlated with demographic and physiological information with the purpose of predicting treatment outcomes so that more accurate diagnostic recommendation on new cases of traumatic pelvic injuries can be provided.

8.4 Summary

In this chapter first the impact and the importance of the work was described. Then, the main conclusions of the proposed research were described. Finally, the main future work to be conducted as the continuation of the project was outlined.

Appendix A **Snake Model: Illustrating the Evolution of the Initial Curve**

The algorithm for the original Snake model was introduced by Kass et al. in 1988 [21]. The optimal Snake shape and position were defined based on the solution of minimizing the sum of the internal and external energies defined along the Snake. The Snake $S(s)$ is defined as a parameterized curve:

$$S(s) = (x(s), y(s)) \tag{A.1}$$

The curve is evolved such that it minimizes the energy functional:

$$E = \int_0^1 \frac{\alpha}{2}|S'(s)|^2\, ds + \int_0^1 \frac{\beta}{2}|S''(s)|^2\, ds + \int_0^1 \kappa F(S)\, ds \tag{A.2}$$

$F(S)$ is the external energy which is derived from the given image in such a way that it takes smaller values around boundaries. α and β are the parameters that control the curve's tension and rigidity, respectively.

The images presented in Figure A.1 show the evolution of the initial curve in case of the Snake model presented in this dissertation. The results below were produced placing the initial seeds on the outside of the region and letting the Snake be attracted inward, towards the edges. The algorithm needs several tens of iterations to converge, as such the results presented below display the position of the curve after non-consecutive iterations. The upper limit for the number of iterations was set to 65, since the initial seeds are placed relatively close to the boundary. If they exist, the changes in placement of the curve after this number of iterations are not significantly improving

the results.

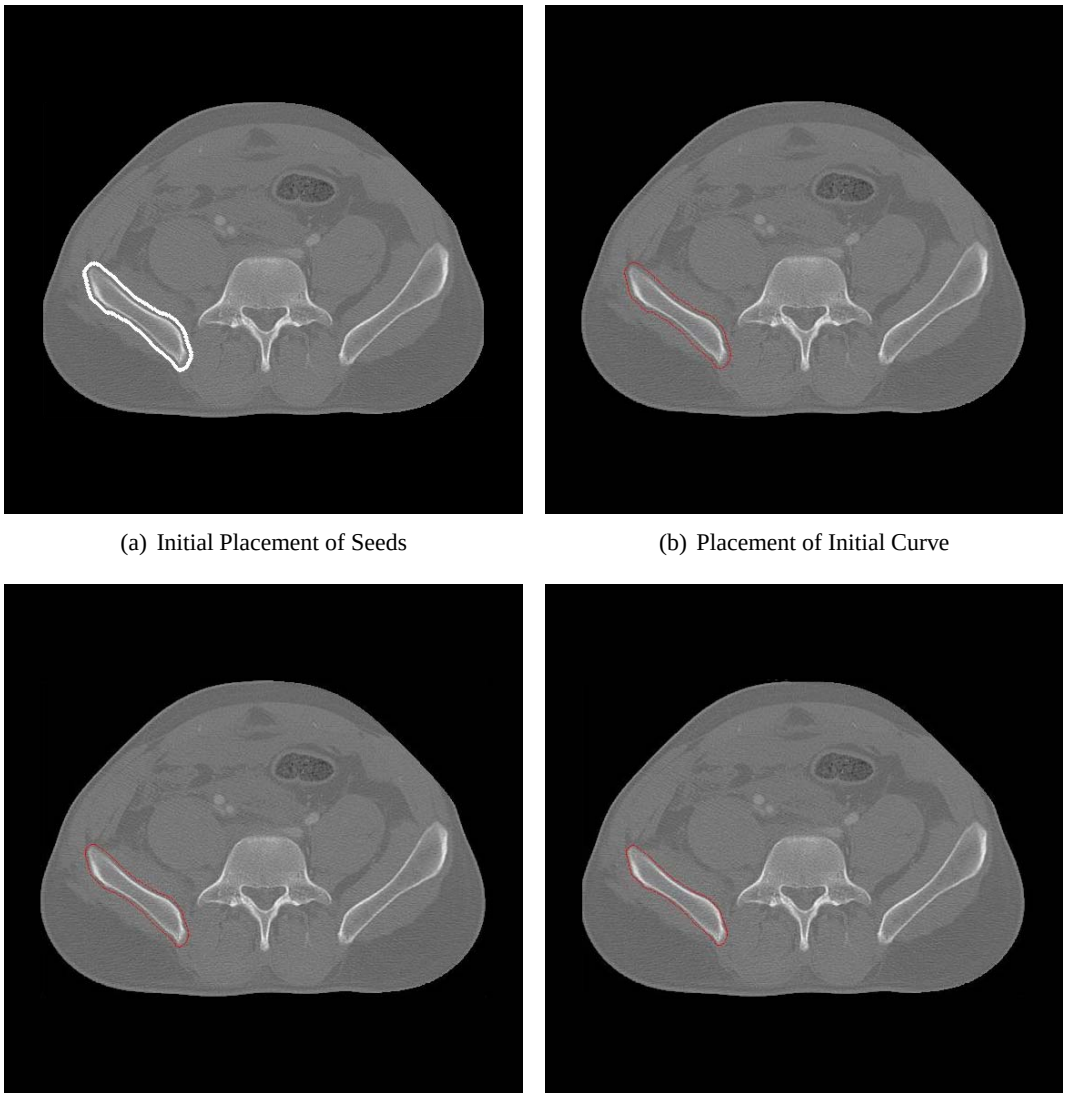

(a) Initial Placement of Seeds

(b) Placement of Initial Curve

(c) Placement of Curve at Iteration 16

(d) Placement of Curve at Iteration 28

Figure A.1: Snake Model: Illustrating the Evolution of the Initial Curve

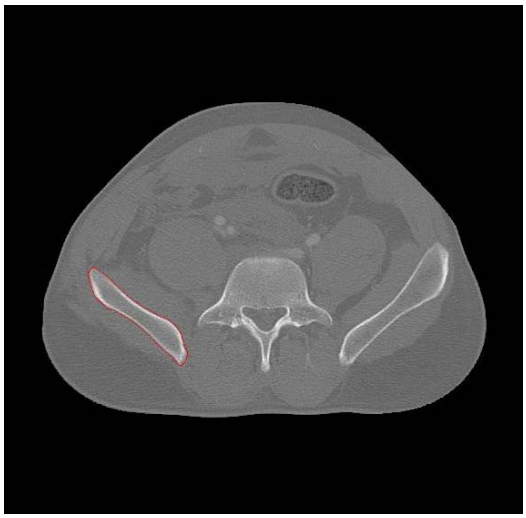

(e) Placement of Curve at Iteration 40

(f) Placement of Curve at Iteration 58

(g) Final Convergence of the Snake

Figure A.1: Snake Model: Illustrating the Evolution of the Initial Curve(Cont.)

Bibliography

Bibliography

[1] R. Adams and L. Bischof. Seeded region growing. *IEEE Transactions on Pattern Analysis and Machine Intelligence*, 16(6), 1994.

[2] B. Barman, S. Mitra, and W. Pedrycz. Shadowed clustering for speech data and medical image segmentation. In *Conference on Rough sets and Current Trends in Computing*, 2008.

[3] S. Belongie, J. Malik, and J. Puzicha. Shape matching and object recognition using shape contexts. *IEEE Transactions on Pattern Analysis and Machine Intelligence*, 24(4), 2002.

[4] Y. Ben-Menachem, D.M. Coldwell, J.W. Young, and A.R. Burgess. Hemorrhage associated with pelvic fractures: causes, diagnosis, and emergent management. *American Journal of Roentgenology*, 157, 1991.

[5] J.C. Bezdek, L.O. Hall, and L.P. Clarke. Review of mr image segmentation techniques using pattern recognition. *Medical Physics*, 20, 1993.

[6] A. Blake, C. Rother, M. Brown, P. Perez, and P. Torr. Interactive image segmentation using an adaptive gmmrf model. In *European Conference in Computer Vision, ECCV*, 2004.

[7] L. Breiman, J.H. Friedman, R.A. Olshen, and C.J. Stone. Classification and regression trees. Wadsworth, Belmont, 1984.

[8] S.S.C. Burnett, G. Strakschall, C.W. Stevens, and Z. Liao. A deformable-model approach to semi-automatic segmentation of ct images demonstrated by application to the spinal canal. *Medical Physics*, 31(2), January 2004.

[9] J. Canny. A computational approach to edge detection. *IEEE Transactions Pattern Analysis and Machine Intelligence*, 8, 1986.

[10] C.J. Carrico, J.B. Holcomb, and I.H. Chaudry. Scientifc priorities and strategic planning for resuscitation research and life saving therapy following traumatic injury: Report of the pulse trauma work group. *Academic Emergency Medicine*, 9(6), 2002.

[11] G. Deng and W. Cahill. An adaptive gaussian filter for noise reduction and edge detection. In *IEEE Nuclear Science Symposium Medical Imaging Conference*, 1993.

[12] F. Ding, W.K. Leow, and T.S Howe. Automatic segmentation of femur bones in anterior-posterior pelvis x-ray images. In *Computer Analysis of Images and Patterns*. Springer Berlin / Heidelberg, 2007.

[13] N. Friedman and S. Russell. Image segmentation in video sequences: A probabilistic approach. In *Thirteenth Conference on Uncertainty in Artificial Intelligence, UAI 97*, 1997.

[14] M. Frucci and G. Sanniti di Baja. Oversegmentation reduction in watershed-based grey-level image segmentation. *International Journal of Signal and Imaging Systems Engineering*, 1, 2008.

[15] M.A. Hall. *Correlation-based feature subset selection for Machine Learning*. PhD thesis, University of Waikato, Hamilton, New Zeeland.

[16] S.Y. Ji, R. Smith, T. Huynh, and K. Najarian. A comparative analysis of multi-level computer-assisted decision making systems for traumatic injuries. *BMC Medical Informatics and Decision Making*, 9(2), 2009.

[17] S. Jiang, W. Chen, Q. Feng, and Z. Chen. Automatic segmentation of cerebral computerized tomography based on parameter-limited gaussian mixture model. In *The 1st International Conference on Bioinformatics and Biomedical Engineering, 2007. ICBBE 2007*, 2007.

[18] A.E. Johnson and M. Hebert. Recognizing objects by matching oriented points. In *IEEE Conference on Computer Vision and Pattern Recognition*, 1996.

[19] P. Kaewtrakulpong and R. Bowden. An improved adaptive background mixture model for realtime tracking with shadow detection. In *2nd European Workshop on Advanced Video Based Surveillance Systems, AVBS01, Video Based Surveillance Systems: Computer Vision and Distributed Processing*, 2001.

[20] D. Kainmueller, H. Lameker, S. Zacow, and H.C. Hege. Coupling deformable models for multi-object segmentation. In *Biomedical Simulation*. Springer Berlin / Heidelberg, 2008.

[21] M. Kass, A. Witkin, and D. Terzopoulos. Snakes: Active contour models. *International Journal of Computer Vision*, 1988.

[22] I.Y. Kim and H.S. Yang. A systematic way for regionbased image segmentation based on markov random field model. *Pattern Recognition Letters*, 15, 1994.

[23] J. Kratky and J. Kybic. Three-dimensional segmentation of bones from ct and mri using fast level sets. In *Society of Photo-Optical Instrumentation Engineers Conference Series, SPIE*, volume 6914, April 2008.

[24] C. Lee, S. Huh, T.A. Ketter, and M. Unser. Unsupervised connectivity-based thresholding segmentation of midsagittal brain mr images. *Computers in Biology and Medicine*, 28(3), 1998.

[25] T.H. Lee and R. Komiya M.F.A Fauzi. Segmentation of ct brain images using k-means and em clustering. In *Conference on computer Graphics, Imaging and Vizualization*, 2008.

[26] S. Liu and W. Ma. Seed-growing segmentation of 3-d surfaces from ct-contour data. *Computer Aided Design*, 31(8), 1999.

[27] M. Mancas and B. Gosselin. Towards an automatic tumor segmentation using iterative watersheds. In *Society of Photo-Optical Instrumentation Engineers Conference Series, SPIE*, 2004.

[28] M. Mancas, B. Gosselin, and B. Macq. Segmentation using a region-growing thresholding. In *Society of Photo-Optical Instrumentation Engineers (SPIE) Conference Series*, volume 5672, March 2005.

[29] A. Marakakis, N. Galatsanos, A. Likas, and A. Stafylopatis. A relevance feedback approach for content based image retrieval using gaussian mixture models. In *Artificial Neural Networks ICANN 2006*. Springer Berlin / Heidelberg, 2006.

[30] T. Mcinerney and D. Terzopoulos. Deformable models in medical image analysis: A survey. *Medical Image Analysis*, 1, 1996.

[31] A. Mehnert and P. Jackway. An improved seeded region growing algorithm. *Pattern Recognition Letters*, 18(10), 1997.

[32] G. Mori, S. Belongie, and J. Malik. Efficient shape matching using shape contexts. *IEEE Transactions on Pattern Analysis and Machine Intelligence*, 27(11), November 2005.

[33] NIH. Burns ans traumatic injury fact sheet. National Institutes of Health - http://www.nih.gov/about/researchresultsforthepublic/BurnsandTraumaticInjury.pdf.

[34] S. Osher and J.A. Sethian. Fronts propagating with curvature dependent speed: Algorithms based on hamilton-jacobi formulations. *Computational Physics*, 79(1), 1988.

[35] Z. Peter, V. Bousson, C. Bergot, and F. Peyrin. A constrained region growing approach based on watershed for the segmentation of low contrast structures in bone micro-ct images. *Pattern Recognition*, 41(7), 2008.

[36] Z .Peter, Z. Bousson, C. Bergot, and F. Peyrin. Segmentation of low contrast features in bone micro-ct images by a constrained region growing approach based on watershed. In *4th IEEE International Symposium on Biomedical Imaging: From Nano to Macro, 2007. ISBI 2007*, April 2007.

[37] T.D. Peterson, M.J. Mello, K.B. Broderick, P.L. Lane, L.A. Prince, A. Jones, and P.E. Goodman. Trauma care systems 2003, 2003. American College of Emergency Physicians.

[38] D.L. Pham, C. Xu, and J.L. Prince. Current methods in medical image segmentation. *Annual Review of Biomedical Engineering*, 2(1), 2000.

[39] R. Pohle and K.D. Toennies. Segmentation of medical images using adaptive region growing. In *Society of Photo-Optical Instrumentation Engineers (SPIE) Medical Imaging*, 2001.

[40] J.R. Quinlan. C4.5: Programs for machine learning. Morgan Kaufmann Publishers, 1993.

[41] O.G. Rousset and H. Zaidi. Correction for partial volume effects in emission tomography. In *Quantitative Analysis in Nuclear Medicine Imaging*. Springer US, 2006.

[42] A. Sarkar, M.K. Biswas, and K.M.S. Sharma. A simple unsupervised mrf model based image segmentation approach. *IEEE Transactions on Image Processing*, 9, 2000.

[43] T.B. Sebastian, H. Tek, J.J. Crisco, and B.B. Kimia. Segmentation of carpal bones from ct images using skeletally coupled deformable models. *Medical Image Analysis*, 7, 2003.

[44] D. Sen and S.K Pal. Image segmentation using global and local fuzzy statistics. In *2006 Annual IEEE India Conference*, September 2006.

[45] Mehmet Sezgin. Survey over image thresholding techniques and quantitative performance evaluation. *Journal of Electronic Imaging*, 2004.

[46] W. Shi, L. Mei, A. Darzi, and P. Edwards. Semi-automated segmentation of pelvic organs for ar guided robotic prostatectomy. In *Conference on Medical Image Computing and Computer Assisted Intervention*, 2008.

[47] Y. Shi and W.C. Karl. A real-time algorithm for the approximation of level-set-based curve evolution. *IEEE Transactions on Image Processing*, 17(5), 2008.

[48] R. Shojaii, J. Alirezaie, and P. Babyn. Automatic lung segmentation in ct images using watershed transform. In *IEEE International Conference on Image Processing*, 2005.

[49] A. Souza, J.K. Udupa, and P.K. Saha. Volume rendering in the presence of partial volume effects. *IEEE Transactions on Medical Imaging*, 24(2), 2005.

[50] F. Spitzer. Markov random fields and gibbs ensembles. *Amer. Math.*, 78, 1971.

[51] J.V. Stough, R.E. Broadhurst, S.M. Pizer, and E.L. Chaney. Clustering on local appearance for deformable model segmentation. In *Symposium on Biomedical Imaging: From Nano to Macro*, 2007.

[52] J.V. Stough, R.E. Broadhurst, S.M. Pizer, and E.L. Chaney. Regional appearance in deformable model segmentation. In *Information Processing in Medical Imaging*. Springer Berlin / Heidelberg, 2007.

[53] M. Straka, A. LaCruz, A. Kochl, M. Sramek, D. Fleischmann, and E. Groller. 3d watershed transform combined with a probabilistic atlas for medical image segmentation. In *Proceedings of MIT 2003*, 2003.

[54] E. Street, L. Hadjiiski, B. Sahiner, S. Gujar, M. Ibrahim, S.K. Mukherji, and H.-P. Chan. Automated volume analysis of head and neck lesions on ct scans using 3d level set segmentation. *IEEE Transactions on Image Processing*, 34(11), November 2007.

[55] M. Suk. A new image segmentation technique based on partition mode test. *Pattern Recognition*, 16, 1983.

[56] C. Tang, D.D. Blatter, and D.L. Parker. Correction of partial-volume effects in phase-contrast flow measurements. *Journal of Magnetic Resonance Imaging*, 5(2), 2005.

[57] H. Tek and H.C. Aras. Local watershed operators for image segmentation. In *Medical Image Computing and Computer-Assisted Intervention MICCAI 2004*. Springer Berlin / Heidelberg, 2004.

[58] R. Tsai and S. Osher. Level set methods and their applications in image science. *Communications in Mathematical Sciences*, 1, 2003.

[59] UMD. Ciren report: Consequences and costs of lower-extremity injuries, 2005. EMS University of Maryland National Study Center for Trauma - http://www.nhtsa.dot.gov/staticfiles/DOT/NHTSA/NRD/Articles/CIREN-/ConsequencesandCostsofLower-ExtremityInjuries/CIRENReport.pdf.

[60] S. Vasilache, W. Chen, K. Ward, and K. Najarian. Hierarchical object recognition in pelvic ct images. In *The 31th Annual International Conference of the IEEE Engineering in Medicine and Biology Society (IEEE/EMBS)*, 2009.

[61] S. Vasilache and K. Najarian. Automated bone segmentation from pelvic ct images. In *IEEE Bioinformatics and Biomedicine (BIBM) International Workshop on Biomedical and Hearth Informatics (BHI)*, 2008.

[62] S. Vasilache and K. Najarian. A unified method based on wavelet filtering and active contour models for segmentation of pelvic ct images. In *Proceedings of The 2009 IEEE/ICME International Conference on Complex Medical Engineering (CME2009)*, 2009.

[63] S. Vasilache, K. Ward, C. Cockrell, J. Ha, and Kayvan Najarian. Unified wavelet and gaussian filtering for segmentation of ct images; application in segmentation of bone in pelvic ct images. *BMC Biomedical Informatics and Decision Making*, 9, 2009.

[64] R.C. Veltkamp. Shape matching: similarity measures and algorithms. In *International Conference on Shape Modeling and Applications, SMI 2001*, May 2001.

[65] X. Wang and H. Wang. Markov random field modeled range image segmentation. *Pattern Recognition Letters*, 25, 2004.

[66] Q. Xie, X. Chen, L. Ma, and Z. Zhou. Segmentation for ct image based on improved level-set approach. *Congress on Image and Signal Processing*, 3, 2008.

[67] C. Xu and J.L. Prince. Gradient vector flow: A new external force for snakes. In *IEEE Computer Society Conference on Computer Vision and Pattern Recognition*, 1997.

[68] F. Yang and T. Jiang. Pixon-based image segmentation with markov random fields. In *Proceedings of ACCV2002: The 5th Asian Conference on Computer Vision*, 2002.

[69] J. Yao, M. Miller, M. Franaszek, and R.M. Summers. Colonic plyp segmentations in ct colonography-based on fuzzy clustering and deformable models. *IEEE Transactions on Medical Imaging*, 23(11), November 2004.

[70] H.-K. Zhao, S. Osher, and R. Fedkiw. Fast surface reconstruction using the level set method. In *IEEE Workshop on Variational and Level Set Methods, VLSM'01*, 2001.

VITA

Simina Vasilache was born on August 4, 1983, in Bucharest, Romania, and holds Romanian citizenship. She received her Bachelors degree from the Academy of Economic Studies of Bucharest where she studied within the Department of Cybernetics, Statistics and Economic Informatics. Between January 2008 and May 2010 she was employed as a Graduate Research Assistant in the Department of Computer Science at Virginia Commonwealth University.